CRANFIELD UNIVERSITY

MARKEL SAINZ DE LA MAZA GARRASTACHU

PARAMETRIC MODELLING AND FATIGUE DAMAGE ASSESSMENT OF OFFSHORE WIND TURBINE SUPPORT STRUCTURES

SCHOOL OF WATER, ENERGY AND ENVIRONMENT
Advanced Mechanical Engineering MSc

MSc
Academic Year: 2015 - 2016

Supervisor: Dr Athanasios Kolios, Dr Lin Wang
September 2016

CRANFIELD UNIVERSITY

SCHOOL OF WATER, ENERGY AND ENVIRONMENT
Advanced Mechanical Engineering MSc

MSc

Academic Year 2015 - 2016

MARKEL SAINZ DE LA MAZA GARRASTACHU

PARAMETRIC MODELLING AND FATIGUE DAMAGE ASSESSMENT OF OFFSHORE WIND TURBINE SUPPORT STRUCTURES

Supervisor: Dr Athanasios Kolios, Dr Lin Wang
September-2016

This thesis is submitted in partial fulfilment of the requirements for the degree of MSc

ABSTRACT

Offshore wind turbines suffer a number of environmental loads which damage their support structure and decrease their lifetime. These forces are produced by the wind, waves and currents and they damage the monopile cyclically. This project aims to quantify that damage through simulating a parametric FEA (finite element analysis) and by applying Palmgren-Miner's rule. For so, a model has been built in ANSYS Workbench and validated through a modal analysis. Then, the behaviour of a monopile in the Southern North Sea has been simulated: wind speed and wave height data were processed into applicable loads. From the results, the cumulative damage was calculated and lifetime defined. Finally, some parameters were altered to evaluate their influence on the fatigue damage. The parametric modelling and fatigue damage assessment showed, on the one hand, that cathodic protection for monopiles is indispensable and, on the other hand, that the use of larger (thicker, longer and bigger diameter) monopiles improves the lifetime of the structure as damage is reduced.

Keywords:

Monopile, soil, environmental data, mesh, lifetime, cyclic loading.

ACKNOWLEDGEMENTS

I would like to express my deepest appreciation to my supervisors, Dr Athanasios Kolios and Dr Lin Wang, who helped me through the four months the thesis lasted, by giving guidance and advice to fulfil my goals.

I would like to thank my family, as they supported throughout the year, and my friends, especially those I met in Cranfield, because they made my stay here unforgettable as well as my flatmates encouraged me during my daily life.

In addition, I would like to express my gratitude to Borja Solana Santillana who gave me important information about the equations required to calculate water loads; to Mario Cano Diaz, who helped me with wind loading calculations; and finally, to Théo Gentils, who helped me with some problems I had to face to make my *ANSYS Workbench* simulations work correctly.

TABLE OF CONTENTS

LIST OF FIGURES

LIST OF TABLES

LIST OF EQUATIONS

1 INTRODUCTION

Wind energy has been used since ancient times using its mechanical power in windmills (Persians) [1] or for transportation (sailing), among others. The finiteness of fossil fuel reserves as well as the contamination while burning them made some people look at other alternatives to produce power. Wind can be found everywhere on Earth, and, consequently, the use of wind as an energy source was worth developing. The first political will to implement this idea appeared in the United States, Denmark and Germany. During the 20th century a number of wind turbines were built and assessed; analysing different sizes and types (horizontal axis, vertical axis, two blades, three, etc.) [2]. Although nowadays there is more than one kind of aerogenerators in use, the 'Danish' wind turbine was proved to be noticeably successful at generating electricity. This turbine consists of a three-bladed rotor and performs at a constant speed [3].

In order to generate power at large-scale, a significant number of wind turbines are placed together, creating wind farms. On-shore farms usually require a lot of space and that can be a problem, even more if the best spots are already taken [4]. Therefore, a solution must be found and the sea happens to be the perfect one. Apart from having plenty of space, sea wind is stronger and more frequent, which makes offshore wind turbines more productive [1]. However, some challenges such as electricity transport or supporting turbines must be faced. The last one is the main topic of this thesis and in which we will focus on.

The support structure of an offshore wind turbine is the structure which goes from the sea level to the seabed, introducing itself on it several meters. Its type and dimensions depend on the mainly in the wind turbine location. The place in which it is placed will define the expected loads and tides, making the structure more robust or larger. The support structure suffers a variety of loads such as waves and currents. Moreover, wind hitting the turbine and tower generates a moment on it and all these loads must be transferred to the soil. Therefore, soil characteristics and its connection to the turbine become really important [5]. However, the characteristic which defines the support structure type is the water

depth. Depending on it the structure could be floating on the sea (depths > 50m), a multipod (25-50m) or a monopod (< 25m) [5] [6]. In case of using monopod structures, there is a single interface with the seabed, whereas multipods have three or four interfaces:

- **Gravity foundations:** It is simple structure for shallow waters with a large base which transmits loads to the soil. Its base is made by reinforced concrete and has enough self-weight (1400-3000 tones) to avoid overturning. They are built onshore and installed offshore after being filled with gravel and sand. In spite of requiring little time to be installed, calm weather is necessary for so. Nevertheless, they are cheap and have been proven to be cost-effective, although their effectiveness is limited to not inclined seabed. [5]
- **Monopile:** It is the most common structure. The monopole is a simple structure which works as an extension of the tower, joining it with the seabed and introducing itself inside the soil. It also has a transition piece linking the tower and the pile. As long as it is a two pieced structure and light compared to others (usually < 250 tones), installation is fast and low risk are taken due to be a well-known concept. However, hydraulic hammer installation can affect environmental concerns and drilling (slower and more expensive) is required in some sites. Moreover, the cost of steel and fabrication can be relatively high. [5]
- **Monopod bucket foundation:** The monopod bucket foundation is the structure “between” monopoles and gravity foundations which performs cost-effectively in certain soil conditions. It can combine several installation methods avoiding the use of expensive machinery. Furthermore, less steel than in monopiles is required. However, fabrication is more expensive as the structure is complex and installation risks are higher. [5]
- **Multipods:** The main difference with monopods lays on the moment transference to the soil, which is obtained by tension/compression actions. The gravity, piled and caisson based multipods are the most common ones and they are used in 25-50m deep seas. Often utilized in

oil and gas industries, they have not been implemented in offshore wind farms. Their size and geometry varies as well as the material or number of legs. The necessary stiffness to resist the moment is obtained through the addition of steel to the structure. Although they can fulfil structural requirements and installation can be fast, there are lots of logistic problem which, together with the increase of the cost due to welding, tend to make them highly expensive. [5]

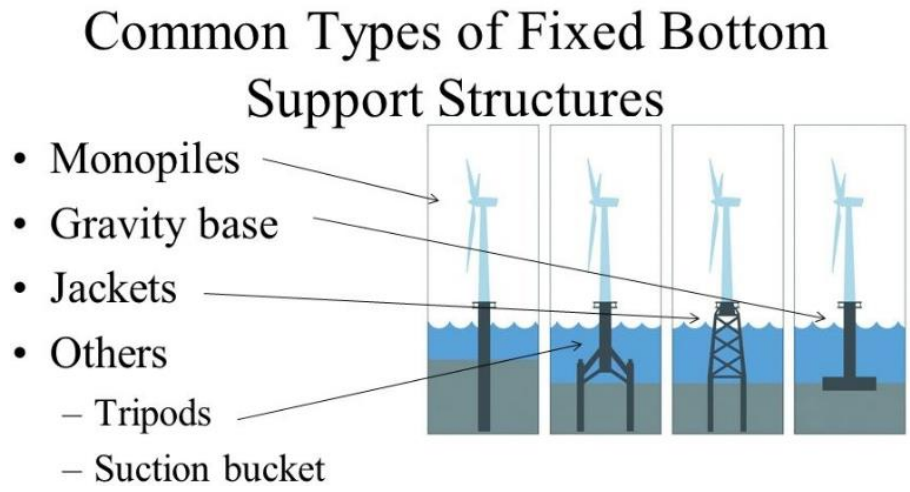

Figure 1-1 Common Offshore Wind Turbine Support Structures [7]

Finally, bear in mind that there are floating structures for 50m < depths, although they are not explained in this paper. What is more, this study aims to analyse the performance of a monopile under cyclic environmantal loads. Furthermore, one of the important aspects of later study is soil-monopile interaction. However its behaviour can be modelled in different ways (*Appendix B.1 Soil*), the present paper uses a large cylinder with soil properties as explained in *3.1 Soil* to simulate the seabed while the monopole is cyclically loaded.

Due to this loads, during their lifetime, offshore structures are continuously accumulating damage, which varies depending on the environment they are placed. They suffer “random” wind and wave loads as well as current forces. This arbitrary forces slowly alter the structural stiffness, damping and natural frequencies among others and can cause fatigue damage, which could end up with the structure collapsing. Moreover, in spite of the unpredictability of marine

loads, uncertainties of the structure must be taken into account. Small notches can propagate after the structure having suffered cyclic loads and create cracks, which will grow until a fracture occurs. Therefore, some damage detection methods have been developed, so that it can be fixed before a failure occurs. [8] [9]

The traditional way of assessing the damage on the offshore structure is by visual inspection. However, this method can be risky, difficult and costly for a structure placed in the sea. Consequently, new techniques have been developed in order to avoid these limitations and making damage detection faster and more effective from an economical point of view. One of them is through analysing the vibration modes. As it was previously commented, structural damage leads to an alteration of natural frequencies of the structure and doing a vibration based inspection these changes can be assessed and damage location and severity determined. [8] [10]

Despite damage detection is really important, this paper aims to analyse the behaviour of a structure under periodic loads. Uncertain loads in marine structures produce oscillatory stresses in structural elements which lead to fatigue at stress concentration points, such as notches and cracks [9]. To simulate and evaluate the fatigue in the structure, a number of cases have been applied to the monopile model built in ANSYS Workbench. From them, stress amplitudes were obtained, which (using S-N curves) are used to obtain the cumulative damage through Palmgren-Miner's rule; and, therefore, lifetime.

- **Palmgren-Miner rule** is a simple cumulative damage model which widely use. Suppose a structure can tolerate a concrete number of cycles at each stress level. If the load cycles are less than maximum number the structure can withstand, it will not fail. Once it suffers that amount of damage, we can say that it has consumed a proportion of life. This is called D, the damage suffered by the structure. If several cycles are applied at different stress levels, the damage received from each stress level can be calculated and added, getting a cumulative damage in this way. [11]

$$\sum_{i=1}^{k} D_i = \sum_{i=1}^{k} \frac{n_i}{N_i} = D \qquad \textbf{(1-1)}$$

Where:

k: $number\ of\ stress\ levels\ applyed$
D_i: $damage\ received\ at\ stress\ level\ number\ i$
D: $accumulated\ damage$
n_i: $number\ of\ cycles\ which\ suffered\ at\ stress\ level\ number\ i$
N_i: $maximum\ number\ of\ cycles\ which\ can\ be\ suffered\ at\ stress\ level\ number\ i\ without\ fatigue\ damage$

If the D is more than 1, then, the structure will fail before completing the load cycle. On the other hand, N_i is obtained from S-N curves (**Figure 1-2**). This lines represent the maximum number of cycles which can be withstand without failure. The area on the right (and above of line) contains the points (stress and number of cyles) in which failure will occur while the left-bottom area is the “safe” area. Depending on the material and notches this curves will vary, they will be lower in case of being any imperfection.

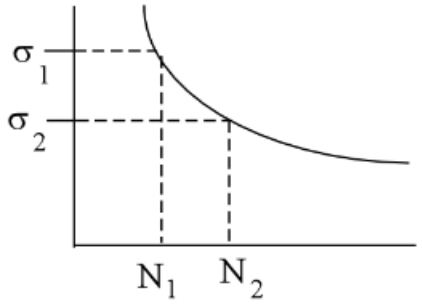

Figure 1-2 S-N curve example

So, by estimating lifetime and how cyclic loads damage the structure, periodical inspections can be performed to repair small notches and cracks, avoiding the collapse of the structure or fatigue failure. Furthermore, a parametric analysis has been carried out to evaluate how fatigue behaviour can be improved by modifying some parameters.

2 LOAD CALCULATION OF OFFSHORE WIND TURBINE SUPPORT STRUCTURES

A monopile structure suffers both static and cyclic loads. On the one hand, it has to withstand the weight of the tower and rotor-nacelle assembly as well as its own one. On the other hand, fluid loads (wind and water) affect the structure. Waves and tides are cyclic loads on the monopile, while the wind hits both tower and blades, and these forces must be transmitted to the seabed through the support structure. This part aims to explain how to process environmental data (wind speed, wavelength and period, and so on) into loads applicable to the model.

2.1 Wind Loading

The only wind data necessary for this analysis is the speed; the direction is not required as wind load is applied in the most unfavourable direction (same direction as waves) Wind speed is measured at 10 m height and an hourly mean is determined. Although the wind has an effect on the current speed, it only affects directly the tower and the rotor-nacelle assembly in the structure.

2.1.1 Wind Profile

Calculation of wind load on the tower has three main parts: wind profile (wind speed variation along the height), wind pressure and application of that pressure on the tower. The required data for future calculus is the speed over the whole height of the tower; therefore, normal wind profile model (NWP) is applied [12]:

$$V(z) = V_{10}\,(z/z_{10})^{\alpha} \qquad \textbf{(2-1)}$$

Where:

$V(z)$: $speed\ at\ z\ [m\ /\ s]$
V_{10}: $speed\ at\ the\ measuring\ height\ z_{10}\ [m\ /\ s]$
z: $height\ [m]$
z_{10}: $height\ of\ 10\ [m]$
α: $power\ law\ coefficient\ (0.014)\ [-]$

As an example, if measured wind speed at 10 m were 15 m/s, wind velocity profile would look like in **Figure 2-1**:

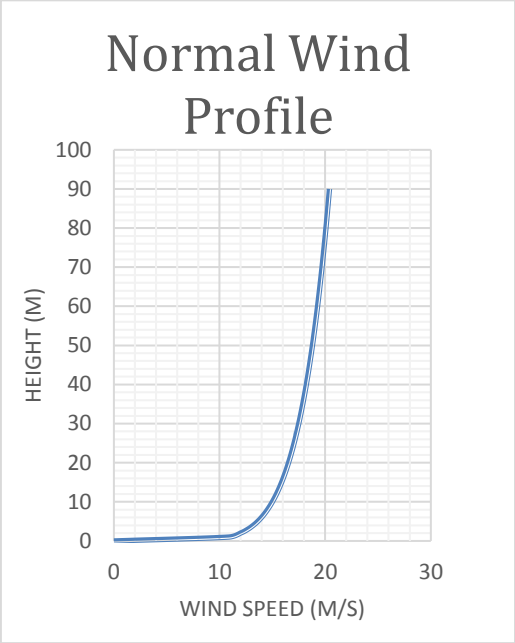

Figure 2-1 NWP example

In order to apply loads to the Workbench geometry, a mean velocity must be calculated for each body. For so, the mean was calculated for each 5 m high part, keeping in mind that the last one was 7.6 m tall. Results are shown in *Appendix A.1 Normal Wind Profile on Tower Bodies*.

2.1.2 Wind Pressure

Once obtained wind speed at each height, wind pressure is calculated in the following way [13]:

$$p_w = \frac{1}{2}\,\rho_{air}\,{V_{wind}}^2 \qquad \textbf{(2-2)}$$

Where:

$$\rho_{air}: air\ density\ [kg/m^3]$$
$$V_{wind}: wind\ speed\ [m\ /\ s]$$

2.1.3 Application of Wind Load on the Tower

There are two ways of applying this force on the tower.

The first and the easiest is applying a drag coefficient (C_D=1.2 [14]):

$$F_{wind} = p_w \, A \, C_D \tag{2-3}$$

Where:

$$A: projected\ area\ of\ the\ tower\ [m^2]$$

However, there is another one which takes into account the distribution of the pressure along the tower circumference, which, according to [15] is the shown in **Figure 2-2**:

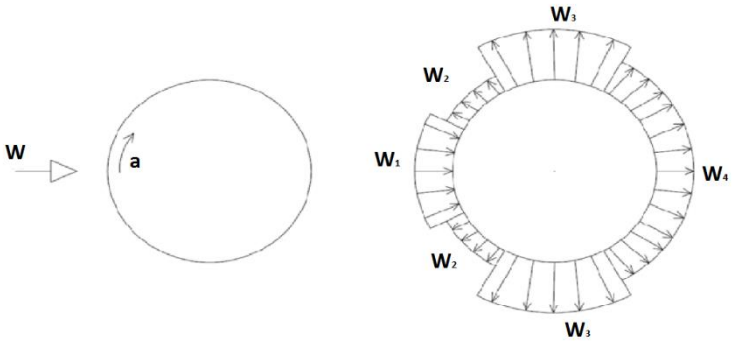

Figure 2-2 Wind pressure distribution along the circumference of the tower [15]

Where w is the pressure multiplied by a coefficient:

$$w = \begin{cases} w_1 = p_w & [0 \div 30°] \\ w_2 = 0.6\, p_w & [30 \div 60°] \\ w_3 = 1.85\, p_w & [60 \div 120°] \\ w_4 = 0.7\, p_w & [120 \div 180°] \end{cases} \tag{2-4}$$

In both cases, the calculus must be done for each body of the tower as loads are applied on each.

In the end, it was decided to use the first solution as the tower is not a subject to study, and only forces transmitted to the monopile are of any interested for this study. Furthermore, if the resultant of pressures in **Figure 2-2** is calculated (taking into account the coefficients in the equation above and the application angle of w_1, w_2, w_3 and w_4) getting a $1.05 * p_w \approx p_w$, so it has no major influence in monopole behavior as the forces transmitted from the tower are almost the same.

2.1.4 Wind Load on Rotor-Nacelle Assembly

Load on the rotor can be calculated using the BEM (Blade Element Momentum) theory [5]. This is an iterative process which determines forces on the blade by combining Blade Element theory and Momentum theory. However, a detailed calculation of thrust on the tower is not one of the goals of this thesis, therefore, it was decided to apply some thrust coefficients (**Figure 2-3**) to obtain the load on the rotor.

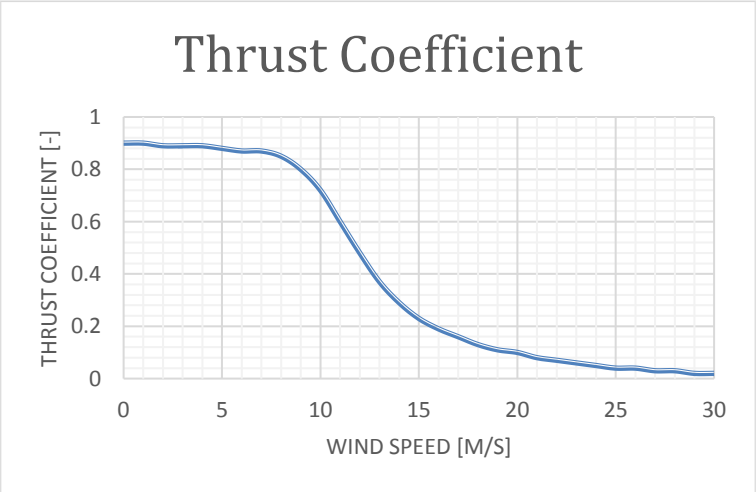

Figure 2-3 Thrust coefficient vs Wind speed [16]

The graph shows a decrease of thrust coefficient when wind speed becomes higher. This means that thrust force does not necessarily get higher along with wind speed. Next equation shows how thrust is calculated [17]:

$$T = \frac{1}{2}\,\rho_{air}\,A\,C_T\,{V_{wind}}^2 \qquad \textbf{(2-5)}$$

Where:

ρ_{air}: $air\ density\ [kg/m^3]$
V_{wind}: $wind\ speed\ [m\ /\ s]$
A: $area\ covered\ by\ turbine\ blades\ [m^2]$
C_T: $thrust\ coefficient\ [-]$

Nevertheless, in case of wanting a more detailed calculation of forces (thrust and torque) on the turbine BEM (blade element momentum) theory can be

followed, which is explained in *Appendix A.2 Wind Load on Rotor-Nacelle Assembly (BEM)*.

2.2 Waves and Currents

This part aims to calculate loads on the monopile due to seawater movement. Water particle velocity is calculated as explained below for current and waves. Once so is done, force is determined along the depth.

2.2.1 Currents Velocity Profile

There are many local or global parameters affecting currents, but current velocity changes very slowly so that a mean speed can be taken and applied for the whole fatigue analysis. However, its variation with depth must be calculated in which current created by the wind is also taken into account [12]:

$$U_c(z) = U_{c,sub}(z) + U_{c,wind}(z) + U_{c,surf}(z) \quad \textbf{(2-6)}$$

Where:

$$U_c(z): total\ current\ velocity\ at\ level\ z\ [m/s]$$
$$z: distance\ from\ still\ water\ level, positive\ upwards\ [m]$$
$$U_{c,sub}(z): subsurface\ current\ velocity\ at\ z\ [m/s]$$
$$U_{c,wind}(z): wind-generated\ current\ velocity\ at\ z\ [m/s]$$
$$U_{c,surf}(z): wave\ induced\ current\ velocity\ at\ z\ [m/s]$$

Although $U_{c,surf}$ is 0 (it is for breaking wave zone, which is near the coast), the other speeds are calculated this (taking into account that the depth is 20 m):

$$U_{c,sub}(z) = U_{c,sub}\left(\frac{d+z}{d}\right)^{1/7} \quad \textbf{(2-7)}$$

Where:

$$U_{c,sub}: subsurface\ current\ velocity\ at\ still\ water\ level\ [m/s]$$
$$d: depth\ to\ still\ weater\ lever, taken\ positive\ [m]$$

And wind-generated current:

$$U_{c,wind}(z) = U_{c,wind}\left(\frac{d_0 + z}{d_0}\right) \quad \textbf{(2-8)}$$

Where:

d_0: $depth\ from\ still\ water\ level\ to\ seabed\ [m]$

$U_{c,wind}$: $0.015\ u(10\ m, 1\ hour)$

$u(10\ m, 1\ hour)$: $hourly\ mean\ wind\ speed\ at\ 10\ m\ heigh\ [m/s]$

Figure 2-4 is an example of current velocity profile, for $U_{c,sub} = 0.9\ m/s$ and $u(10\ m, 1\ hour) = 7\ m/s$:

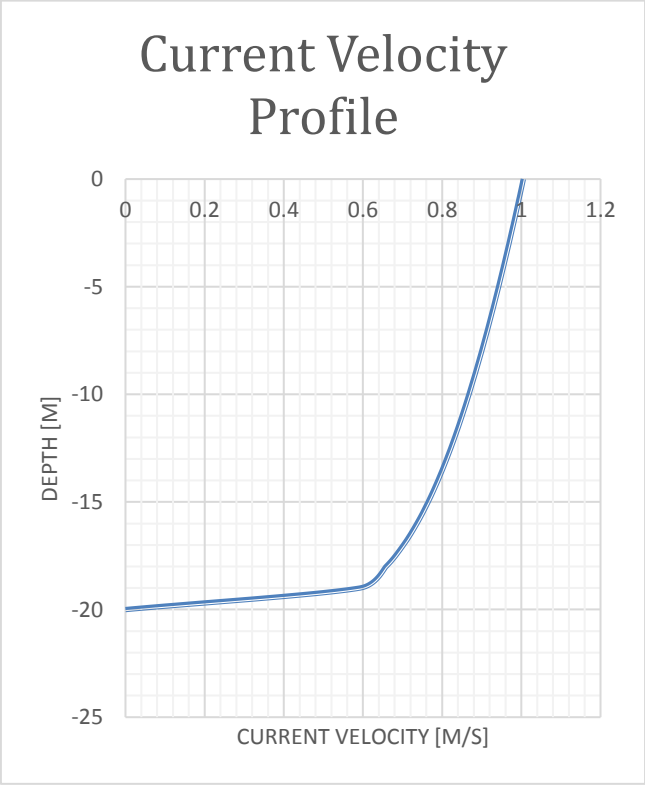

Figure 2-4 Current Velocity Profile example

2.2.2 Waves Particle Cinematics

To determine water particle velocity due to waves, airy theory was followed [14], but first, wavelength must be calculated [18]:

$$\lambda_{wave} = \frac{g\ T^2}{2\ \pi} \quad \textbf{(2-9)}$$

Where:

$$g: gravity\ (9.81\ m/s^2)$$
$$T: wave\ period\ [s]$$

Period must be calculated before the wavelength. For so, *steepness* is necessary, which will be constant for all the calculus and it will have a value of 1/40 [18]:

$$T = \sqrt{(2\pi\ H)/(g\ Steepness)} \quad \textbf{(2-10)}$$

Where:

$$H: wave\ height\ [m]$$
$$Steepness: wave\ height\ divided\ by\ wave\ length\ [-]$$

Once wavelength is determined, the airy theory can be applied. Particle velocity and acceleration are calculated in the next way:

$$u(x,z,t) = \xi\ 2\ \pi\ f\ \frac{\cosh k_{wave}\ (z+d)}{\sinh k_{wave}\ d}\ \cos(k_{wave}\ x - 2\ \pi\ f\ t) \quad \textbf{(2-11)}$$

$$\dot{u}(x,z,t) = \xi\ (2\ \pi\ f)^2\ \frac{\cosh k_{wave}\ (z+d)}{\sinh k_{wave}\ d}\ \sin(k_{wave}\ x - 2\ \pi\ f\ t) \quad \textbf{(2-12)}$$

Where:

$$d: water\ depth\ [m]$$
$$k_{wave}: wave\ number = 2\ \pi/\lambda_{wave}\ [-]$$
$$\lambda_{wave}: wave\ length\ [m]$$
$$f: wave\ frequency =\ 1/T\ [Hz]$$
$$\xi: wave\ amplitude = 0.5\ H\ [m]$$
$$H: wave\ height\ [m]$$

Bear in mind that $(k_{wave}\ x - 2\ \pi\ f\ t)$ is the wave phase, therefore, for the calculus next angles have been introduced in radians: 0, π/4, π/2, 3π/4, π, 5π/4, 3π/2, and 7π/4. The water depth will be different in case or been in the crest of the wave or not (which affects also the current profile) and that will be taken into account for the calculation of forces affecting the structure.

2.2.3 Morison Forces

Next step to calculate wave-current loading on the structure is determining Next step is determining drag (C_D) and inertia (C_M) coefficients, as explained in [14], so that Morison equations can be applied to calculate Morison Forces (forces produced due to water particle dynamics). C_D can be calculated based on the drag coefficient for steady flows C_{DS}, which is mainly based on the roughness of the structure surface:

$$C_{DS} = \begin{cases} 0.65 & if\ k/D < 10^{-4} \\ \dfrac{29 + 4\ \log_{10}(k/D)}{20} & if\ 10^{-4} < k/D < 10^{-2} \\ 1.05 & if\ k/D > 10^{-2} \end{cases} \quad \textbf{(2-13)}$$

Where:

$$D: effective\ diameter\ diameter\ of\ the\ structure\ [m]$$
$$k: absolute\ height\ of\ roughmess\ (0.003\ m)$$

C_D is related to C_{DS} through Keulegan-Carpenter number (KC):

$$C_D = C_{DS}\ \psi(C_{DS}, KC) \quad \textbf{(2-14)}$$

Where:

$$KC = 2\ U_m\ T/D$$
$$\psi(KC) = \begin{cases} C_\pi + 0.1\ (KC - 12) & if\ k/D < 10^{-4} \\ C_\pi - 1 & if\ 10^{-4} < k/D < 10^{-2} \\ C_\pi - 1 - 2\ (KC - 0.75) & if\ k/D > 10^{-2} \end{cases}$$
$$C_\pi = 1.50 - 0.024\ (\frac{12}{KC} - 10)$$
$$U_m: maximum\ water\ speed\ along\ the\ wave\ (after\ adding\ current\ velocity)[m/s]$$

Once C_D is calculated, C_M can be determined:

$$C_M = \begin{cases} 2 & KC < 3 \\ \max\{2 - 0.044\ (KC - 3); 1.6 - (C_{DS} - 0.65)\} & KC \geq 3 \end{cases} \quad \textbf{(2-15)}$$

After calculating Morison coefficients forces on the monopile are:

$$f_{Morison}(x, z, t) = f_d(x, z, t) + f_i(x, z, t) \quad \textbf{(2-16)}$$

$$f_d(x,z,t) = C_D \frac{1}{2} \rho_{water} D |u(x,z,t)| u(x,z,t) \quad \textbf{(2-17)}$$

$$f_i(x,z,t) = C_M \frac{\rho_{water} \pi D^2}{4} \dot{u}(x,z,t) \quad \textbf{(2-18)}$$

Where:

$f_{Morison}: hydrodinamic\ load\ [N/m]$
$f_d: hydrodinamic\ drag\ load\ [N/m]$
$f_{Morison}: hydrodinamic\ inertia\ load\ [N/m]$
$\rho_{water}: density\ of\ water\ [kg/m^3]$
$u: water\ particle\ velocity\ [m/s]$
$\dot{u}: water\ particle\ acceleration\ [m/s^2]$
$D: diameter\ of\ cylinder\ section\ [m]$

Calculations are done for different depths and wave phases. Once finished them, an average is calculated for each element (and for each phase) so that a cyclic load can be applied on the Model in *ANSYS Workbench*.

2.3 Load Validation

Validation of wind profile, wind pressure and wave-current loading was carried out by calculating them for the same cases studied in [14]. As the equations used were the same, the results were exactly the same. The only difference was in the wind profile, where this thesis uses 0.014 as a power law coefficient instead of the 0.012 described in the reference, but nothing remarkable. Once it was checked the results were the same. Parameters were changed to our case, higher tower height and 20 m depth.

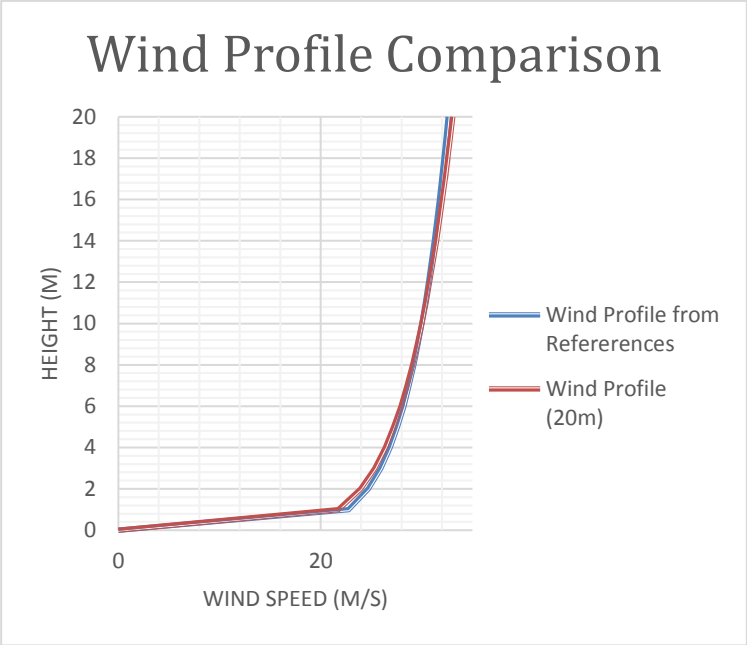

Figure 2-5 Wind Profile Validation

Finally, to validate the thrust, thrust calculus was performed for an 8.02 m/s wind speed and the result compared to the same calculation in [13]. This paper gets 490 kN in that situation while this model gets 460 kN. Although they are not very close, results can be considered good because the calculation method was quite simple and nor the turbine or blade type are the same as in the reference. Therefore, it can be concluded that the load calculation model is validated as the force range is pretty much the same.

More detailed data related to the Validation can be found in *Appendix B.3 Mesh Validation*.

2.4 Load Cases

Environmental data was taken from [18] for the Sothern North sea, number 15631 in **Figure 2-6**.

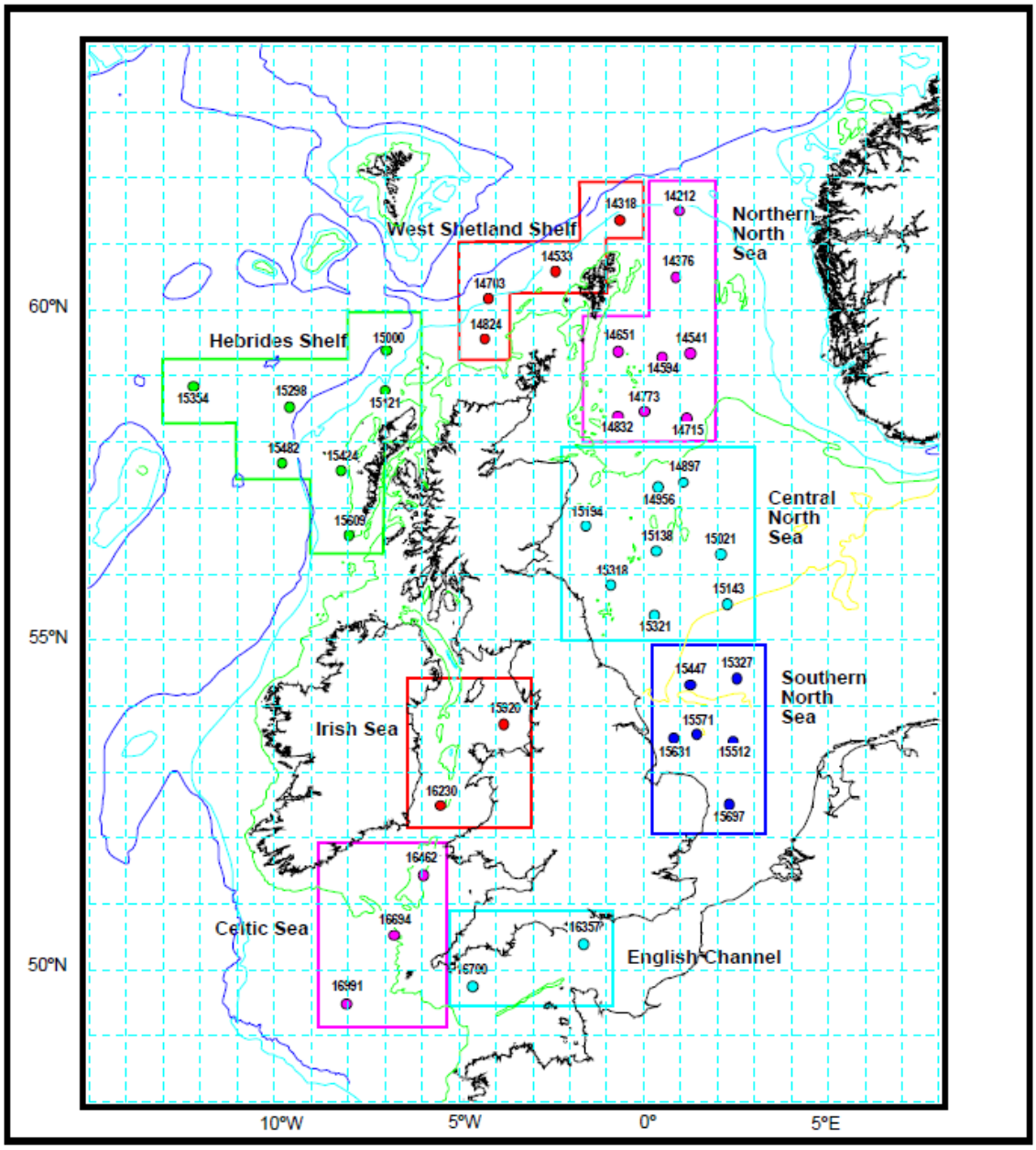

Figure 2-6 Map of the environmental data given in [18]

This standard gives wind speed and wave height distributions used in the simulations. The data used in this simulation is shown in **Figure 2-7**. Simulations were run both with the maximum and mean value of each wind-speed/wave-height range.

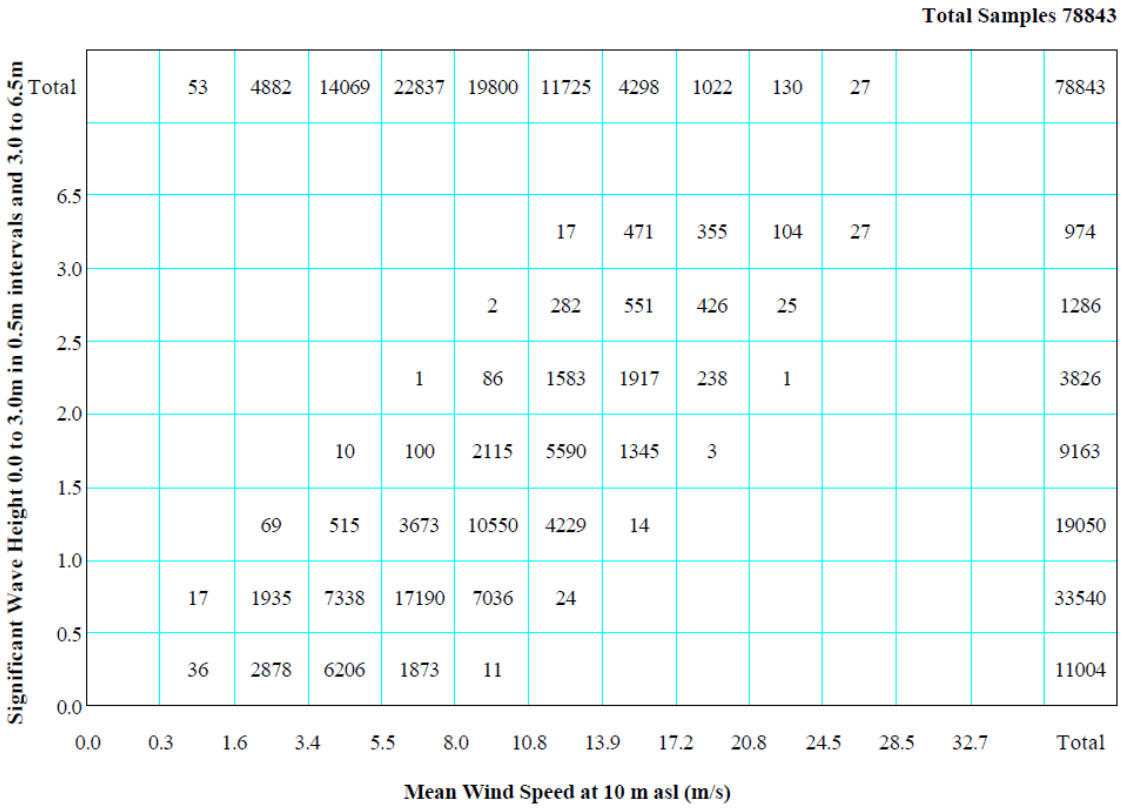

Figure 2-7 Wind speed and wave height distribution in Southern North Sea [18]

3 Parametric Finite element analysis (FEA) model of offshore wind turbine support structures

A parametric FEA model has been established using *ANSYS Workbench* to perform the fatigue damage assessment. This model was divided into two parts: soil and structure. The soil was a large cylinder constituted by several layers of different properties. Besides, the structure was formed by the tower and the support structure.

3.1 Soil Model

The wind turbine aimed to study is placed outside Humber estuary (East of England, Southern North Sea). There, seabed has two clay and one sand layers over a chalk bottom as **Figure 3-1** shows:

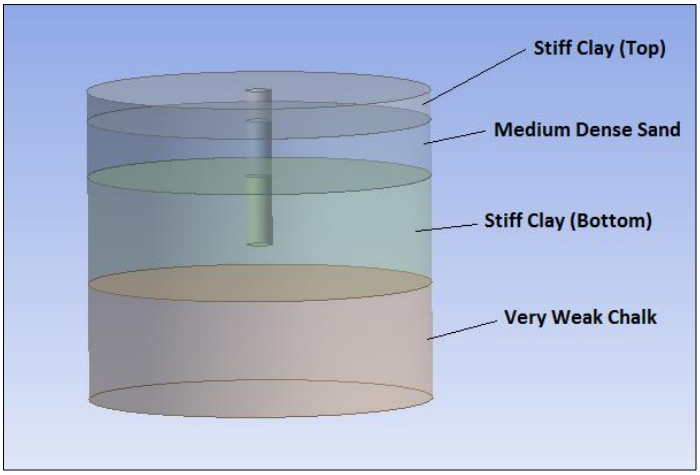

Figure 3-1 Soil Model

Information about layer depth and material was taken from [19]. Then, a large cylinder was created to simulate soil behaviour and, then, material properties (shown in **Table 3-1**) were added. Drucker-Prager Model was used for soil profiles sand and clay.

Material	**Stiff Clay (Top)**	**Medium Dense Sand**	**Stiff Clay (Bottom)**	**Very Weak Chalk**
Density [kg/m^3]	2,000	2,080	2,070	2,100
Young's Modulus [MPa]	10	19	10	-
Bulk Modulus [MPa]	-	-	-	9,000
Poisson's Ratio [-]	0.3	0.3	0.3	0.35
Yield Stress [Pa]	9,700	28,000	9,700	-
Slope [°]	17	30	17	-

Table 3-1 Soil material properties [20] [21]

3.2 Geometry of the Structure

The Structure Model was composed by an 87.6 m tower of variable thickness-diameter and a 56 m height monopile of constant thickness-diameter. It was built following an NREL paper [22], and both bodies were connected by a 'Bonded' connection. **Table 3-2** contains all the dimensions of the structure:

Parameter (m):	**Tower**	**Monopile**
Height	87.6	56
Top Outer Diameter	3.87	6
Top Thickness	0.019	0.05
Bottom Outer Diameter	6	6
Bottom Thickness	0.027	0.05

Table 3-2 Tower and Monopile dimensions [22]

Both parts had been separated in smaller bodies as **Figure 3-2** shows:

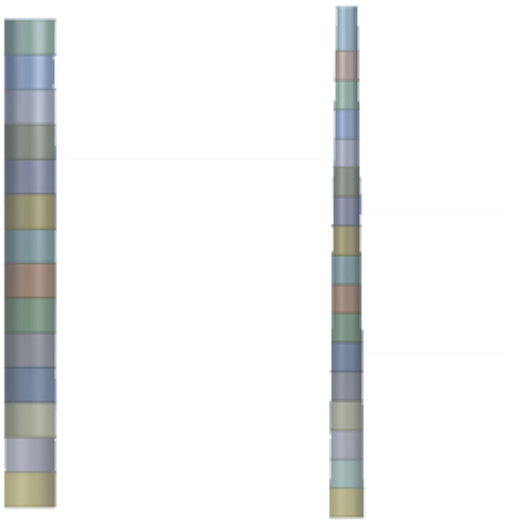

Figure 3-2 The structure by parts: Monopile on the left, Tower on the right (different scale)

The monopile was split into 14 bodies of 4 m; 5 bodies were suffering hydrostatic pressure while the rest were introduced into the seabed (36 m). Their connection to soil was frictional (0.2 friction coefficient) and the structure was able to move by deforming the seabed, but it would work as a dumping system. What is more, a smaller motion amplitude was observed as long as the monopile went deeper into the soil due to the effect of soil. Finally, both monopile bottom edge and soil bottom-lateral surfaces are defined as fixed support in order to prevent the geometry from rigid body motion.

3.3 Mesh Validation

In order to perform a Finite Element Analysis (FEA), a shell mesh was built with quad-type elements. The use of shell elements made it necessary to provide each tower body with a different thickness with the values shown in *Appendix B.2 Tower Thickness*.

To ensure the mesh built was good enough to start the validation, some of its properties were assessed. Aspects to take into account were, on the one hand, Skewness and Orthogonal Quality, both ranged between 0 and 1. Skewness is perfect when it is 0 and a perfect Orthogonal Quality would be all right for 1 [23]. On the other hand, we have Mesh Quality (the better as long as it gets closer to 100%) and aspect ratio, which should be maintained below 10 according to [23]. Before going ahead to validate the mesh, it was ensured that all these parameters had adequate values: smaller Skewness than 0.1, higher Orthogonal Quality than 0.9, aspect ratio below 10 and Mesh Quality over 90% for most of the elements. The tinier were the element sizes introduced, the better were the values obtained. **Table 3-3** shows the results obtained for tower-monopile structure when element size is 0.2m. Graphs related to this properties are shown in *Appendix B.3 Mesh Validation*.

	Element Quality	Aspect Ratio	Skewness	Orthogonal Quality
Nodes	64290	64290	64290	64290
Elements	62824	62824	62824	62824
Min	0.14453	1	5.92E-07	0.15049
Max	0.9964	24.853	0.99724	1
Average	0.98473	1.0852	2.13E-02	0.98775
Standard Deviation	6.33E-02	0.36896	9.06E-02	5.72E-02

Table 3-3 Mesh quality related properties

3.3.1 Modal Analyses

Three analyses were carried out in order to validate the mesh:

- First, the modal frequencies of the tower were obtained. After building the mesh, the simulation was run and modal frequencies got, but only for the tower without Head Mass, which means that rotor-nacelle assembly

is not taken into account. They were compared to the values from [22] and it was observed a convergence while applying smaller element sizes. **Figure 3-3** shows the modal values according to number of elements:

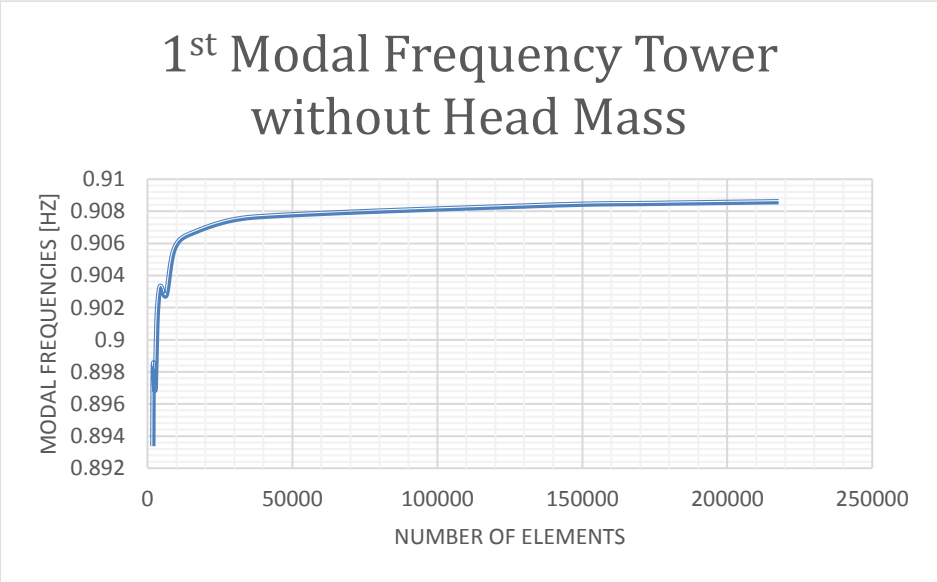

Figure 3-3 1st Modal Frequency vs number of elements, tower without head mass

The graph shows a clear convergence and, although it does not reach 0.8913 Hz, with the last element size simulated the difference is less than 2%. Therefore, the model is good enough for next analysis.

- After introducing a Head Mass, the same simulation was run. The Head Mass is the same one which will be used to simulate the turbine on fatigue analyses and its values are shown in **Table 3-4**.

Rotor Mass	110,000 kg
Nacelle Mass	240,000 kg
Tower Head c.m. offset in upwind direction	0.41 m
Tower Head c.m. vertical offset from tower top	1.97 m
Tower Head moment of inertia about rotor-parallel axis through c.m.	4.37×10^7 kg m^2
Tower Head moment of inertia about lateral axis through c.m.	2.35×10^7 kg m^2
Tower Head moment of inertia about vertical axis through c.m.	2.54×10^7 kg m^2

Table 3-4 Turbine mass and inertia momentums [22]

In this case, 1st modal frequency has to be 0.3188 Hz. Even if that value is not reached the results show a convergence as **Figure 3-4** shows:

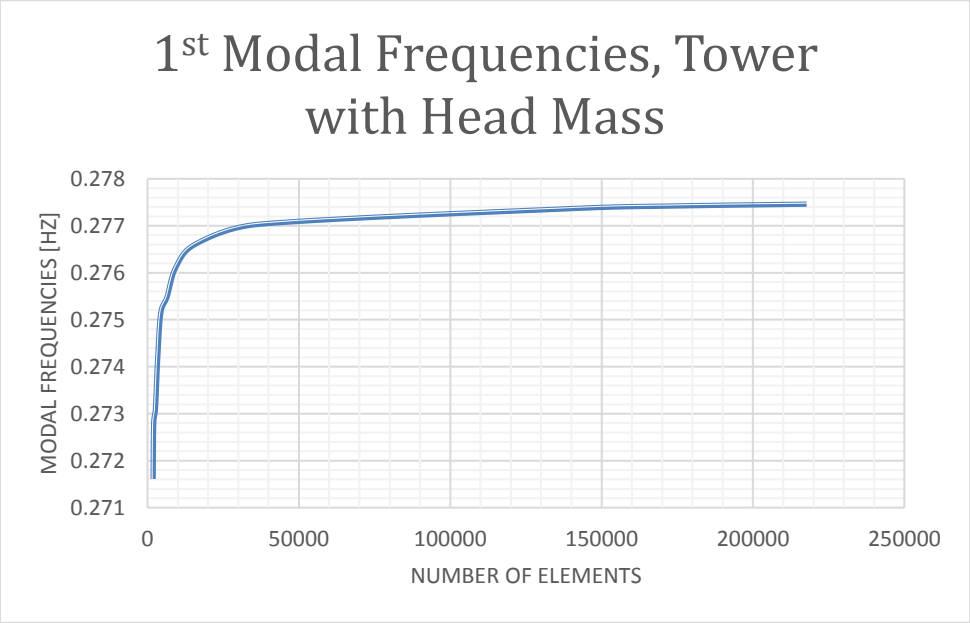

Figure 3-4 1st Modal Frequency vs number of elements, tower with head mass

- Finally, the tower-monopile structure was assessed. The procedure was the same and differences with values from [4] almost the same, as **Figure 3-5** shows:

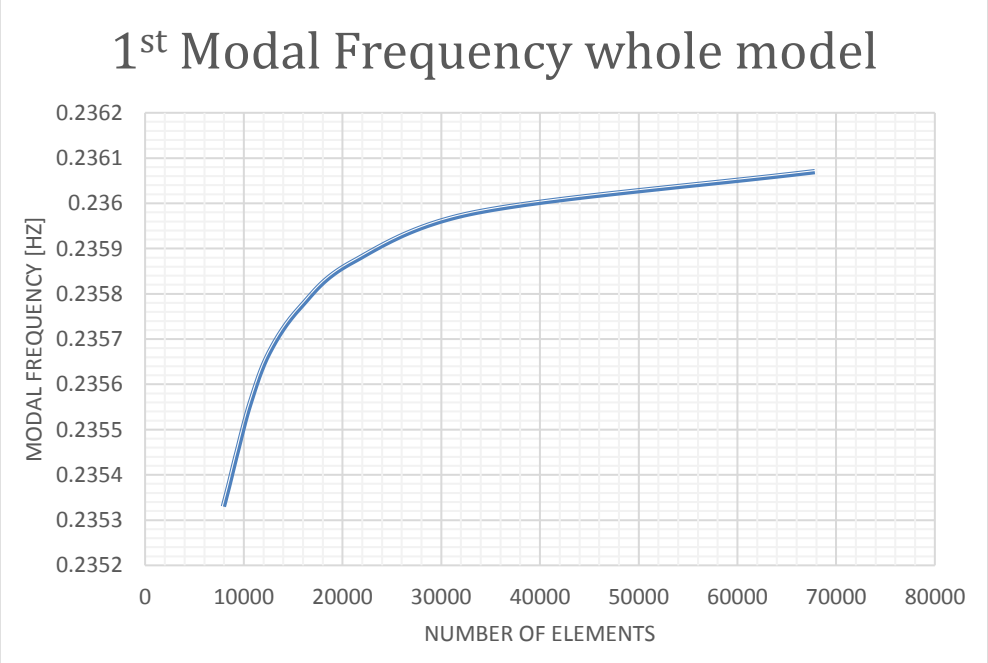

Figure 3-5 1st Modal Frequency vs number of elements, whole model.

Although the differences are not huge (they are shown in *Appendix B.3.1 Modal Analyses*), they are bigger than in the first analyses and they could have its origin in the soil model. Paper [22] shows a spring based soil model while this study uses a large cylinder with seabed characteristics where the monopile is placed. However, the difference with the values from [22] is around 4%, smaller than 5% and consequently good enough for later case studies. What is more, the more elements introduced, the closer the 1st modal frequency is from the value compared to (0.247 Hz).

4 Results

To assess the fatigue damage and perform a parametric analysis of the monopile a number of simulations were performed. A couple of loading cycles were simulated for each case and with the obtained data Palmgren-Miner rule was applied. For so, the monopile point in which the stress range was the highest was evaluated (biggest max-min difference). Therefore, several points were analysed in the first evaluations in order to determine the point which suffers more from fatigue. **Figure 4-1** shows stress for one of the cases. It is observed that maximum stresses are close to the seabed, where contact with soil starts.

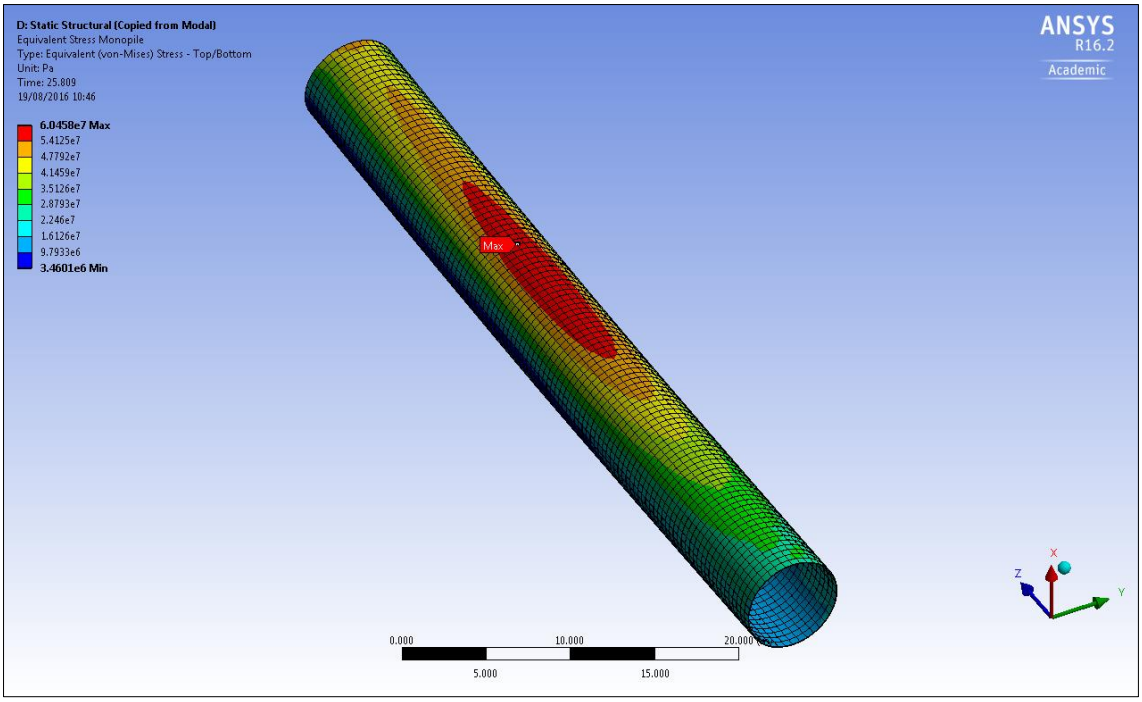

Figure 4-1 Equivalent (Von-Mises) Stress on the monopile.

However, it is not at the point of maximum stress where maximum stress difference on each cycle is located. The study showed it was a several meters below it. It is important to get the stress range if S-N curves (like in **Figure 4-2**) are applied.

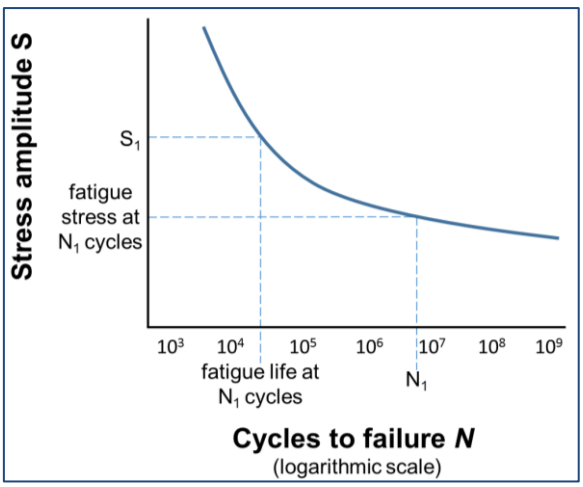

Figure 4-2 S-N curve

Once obtained the stress range (amplitude), next equation [24] is applied to obtain the maximum number of cycles before fatigue failure for each case.

$$log_{10} N = log_{10} a - m\, log_{10} \left(\Delta\sigma \left(\frac{t}{t_{ref}} \right)^{k} \right) \quad \textbf{(4-1)}$$

Where:

$\Delta\sigma$: $stress\ range\ in\ units\ of\ MPa$
$log_{10}\ a$: $intercept\ of\ log\ N\ axis$
N: $fatigue\ life, i.e. number\ of\ stress\ cycles\ to\ failure\ at\ stress\ range\ \Delta\sigma$
t_{ref}: $reference\ thickness, 25\ mm\ for\ welded\ connections\ other\ than\ tubular\ joints, such\ as\ girth\ welds$
t: $thickness\ through\ which\ the\ potential\ fatigue\ crack\ will\ grow$
k: $thickness\ exponent, also\ known\ as\ scale\ exponent$

Table 4-1 shows the coefficients used. Seawater cathodic protection is used in later calculus, although *in air* and *free corrosion* are used in the parametric study to evaluate the necessity of cathodic protection.

Structural detail	***Curve***	***Environment***										
		In air				***In seawater cathodic protection***				***Free Corrosion***		
		log a	***m***	***Range of validity***	***k***	***log a***	***m***	***Range of validity***	***k***	***log a***	***m***	***k***
Butt weld and tubular girth weld, weld toe	*D*	12.164	3	$N<10^7$	0.25	11.764	3	$N<10^6$	0.2	11.687	3	0.2
		15.606	5	$N>10^7$	0.25	15.606	5	$N>10^6$	0.2			

Table 4-1 S-N curves for most frequently used structural details.

4.1 Fatigue Damage Assessment

Load cases shown in **Figure 2-7** are applied in ANSYS Workbench simulations. As load data is given for several wind speeds and wave heights, to calculate the loads and run simulations the maximum of each range has been taken and, later, the same study was performed by taking the mean of each case. Bear in mind that a SCF (Stress Concentration Factor) must be applied to the stress

amplitude as stress concentrations would increase the damage on the structure. This concentrations are due to small notches or imperfections produced during lifetime or during fabrication. According to [25] the minimum value for this factor is 1.5, while no other information is available.

Anyway, for all the simulations, once obtained *N* in each case, the yearly cumulative damage is calculated with the next equation:

$$D_C = \sum_{i=1}^{I} \frac{n_{C,i}}{N_{C,i}}$$

Where:

D_C: $characteristic\ cumulative\ damage$
I: $number\ of\ cases$
$n_{C,i}$: $number\ of\ stress\ cycles\ for\ the\ i^{th}\ case\ (calculated\ with\ the\ percentage\ of\ each\ case\ per\ year\ and\ wave\ period)$
$N_{C,i}$: $number\ of\ cycles\ to\ failure\ at\ i^{th}\ case$

The results showed that the total cumulative damage per year is 0.01025. Since the maximum damage the structure can suffer is 1, the monopile would withstand this loading for 97 years before suffering fatigue failure, which is really good taking into account that offshore wind turbines are designed for 20-30 years [26] [27]. If mean wind speeds and wavelengths for each range are applied, results are even better: 0.00385 cumulative damage and 259 years lifetime. Therefore, it is deduced something obvious, that location is a very important point in fatigue damage design. The study performed was for the Southern North Sea where waves are not expected to exceed 6.5 m. Other zones of the same sea can suffer waves higher than 10 m and, consequently, this same monopile would have its lifetime reduced although it could withstand enough years of loading.

Finally, if a SCF is not applied, lifetime is increased to 740 years. Therefore, it is important to repair stress concentration problems such as notches or cracks as soon as possible as damage is highly increased (from 0.00135 to 0.01025, 659%). Regular inspections can help solving this issue by fixing problems encountered.

4.2 Parametric Analysis

The Parametric Analysis was performed by changing the values of some of the monopile parameters. Furthermore, it was analysed the use of a cathodic protection and the influence of the soil type.

4.2.1 Cathodic protection

Three different S-N curves have been applied: *in air*, *in seawater with cathodic protection* and *free corrosion*. The coefficients for each curve and results are shown in **Table 4-2**. It is observed that cathodic protection makes a huge difference regarding fatigue life.

	Free corrosion	**In air**	**In seawater with cathodic protection**
Cumulative Damage (per year)	0.1102	0.00999	0.01025
Lifetime (years)	9	100	97

Table 4-2 Results with different S-N curves.

4.2.2 Soil type

The Soil Model is composed of sand, clay and chalk layers. This part aims to see the behaviour of the monopile if it was placed into different soils (all layers the same): sand, clay and chalk. Running simulations for all the cases would take too long so only three have being analysed to see the difference between one and other material. These case are the same for all the parametric study (in the parametric study mean wad speed and wave height are used):

1. Wind Speed 4.45 m/s and Wave Height 0.75 m.
2. Wind Speed 9.4 m/s and Wave Height 1.25 m.
3. Wind Speed 15.55 m/s and Wave Height 2.25 m.

Results in **Figure 4-3** show damage for the three analysed cases. While the behaviour for sand and clay is quite similar, chalk soil clearly suffers less damage. The main difference is that sand and clay are granular materials and

their Young's Modulus is lower. Consequently, it can be stated that soils more rigid and higher Young's Modulus are better against fatigue as the soil holds better the monopile and forces are transmitted easier to it.

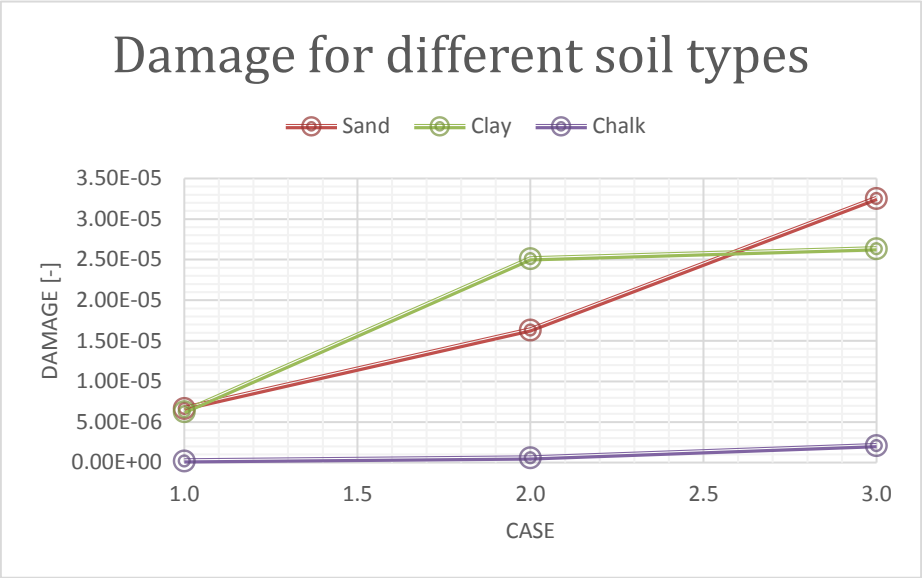

Figure 4-3 Damage according to soil type

For a more detailed analysis, it has been observed that when Young's Modulus gets higher, maximum and minimum stresses go down making the difference between them lower. Therefore, the damage is reduced and monopiles have a longer lifetime.

4.2.3 Thickness

To analyse thickness the three same loading cases were simulated. It was observed how maximum and minimum stress decreased together with thickness increase. The reason why that happens is because the area which has to suffer the stress is larger. Stress is defined as force/surface so, consequently, thickness increase brings a reduction in stresses which ends up in smaller stress amplitudes. As **Figure 4-4** shows, smaller amplitudes obtained through to thicken the monopile reduce the fatigue damage it suffers. Although there have been other parameters analysed, this is probably the best way of improving fatigue damage as it does not suppose a big change regarding installation or assembly with the tower. The main problem (regarding costs)

could be the increase of material used to build it, but it is something that will happen in the case of using a larger diameter or a longer monopile; so, it is not a real problem as these two other solutions require a more material than thickening the structure.

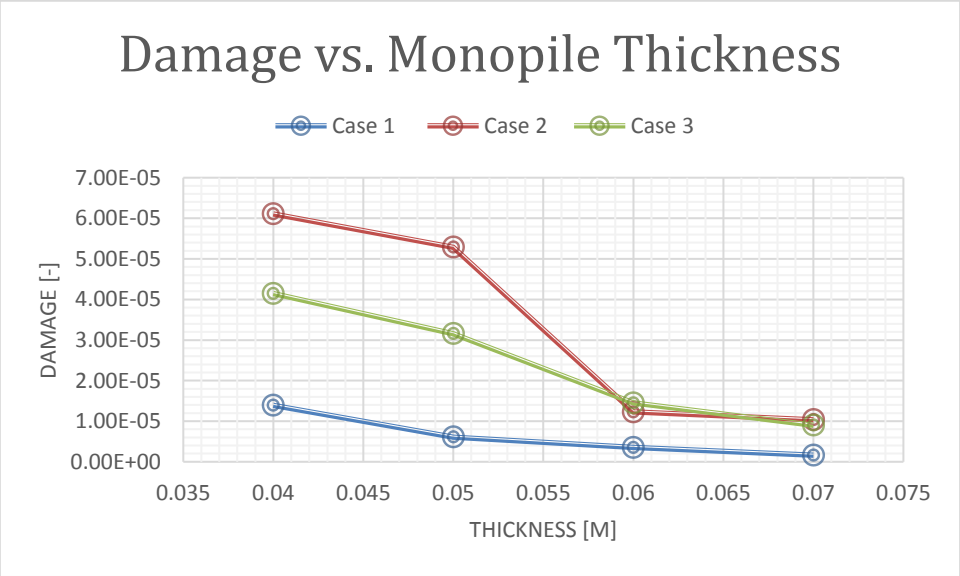

Figure 4-4 Influence of thickness in damage for different cases

4.2.4 Diameter

Increasing the diameter of the monopile is another way of improving lifetime. As it happens with thickness increase, maintaining monopile thickness and increasing its diameter will mean that the section surface would be larger. For the same reason earlier explained, if a force is distributed along a bigger surface, stresses will be lower. Consequently, maximum and minimum stresses are reduced and stress amplitude also decreases. Therefore, damage on the support structure is lower too (see **Figure 4-5**) and lifetime is increased.

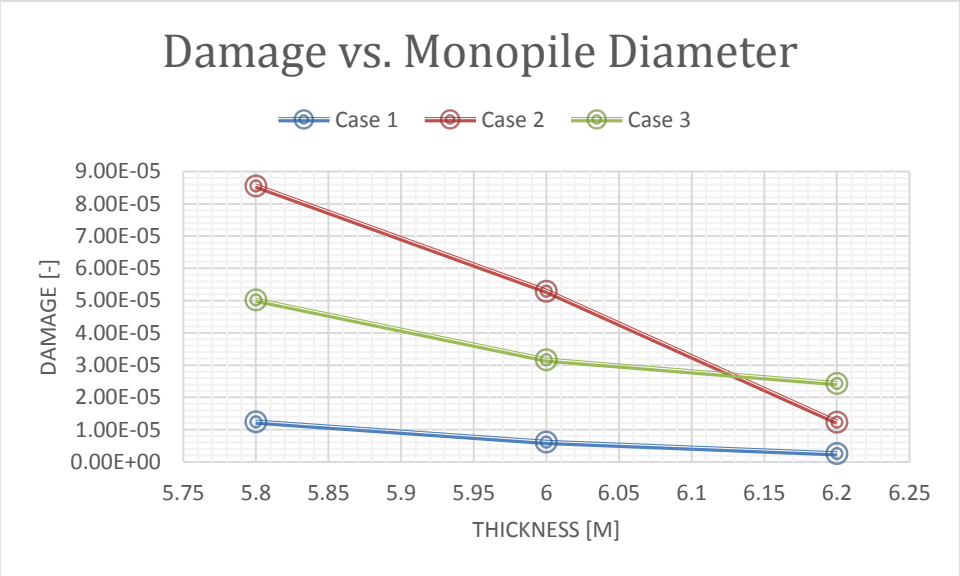

Figure 4-5 Influence of diameter in damage for different cases

The use of a big diameter is not the most suitable option in case of needing fatigue behaviour improvement. A Larger diameter would affect directly the transition piece design and its assembly with the tower. Changing even tower parameters to improve the lifetime of the support structure (remember that this thesis monopile diameter is 6 m and the tower bottom diameter is also 6 m) makes this solution not advisable. Furthermore, installation on the seabed could also change substantially in the case of a monopile with a quite larger diameter.

4.2.5 Length

Longer monopiles also show an improvement regarding damage and lifetime. However, the length is more likely defined by the greatest lateral loadings and the structural stability. Nevertheless, results in **Figure 4-6** show that longer monopiles withstand better cyclic loads along time.

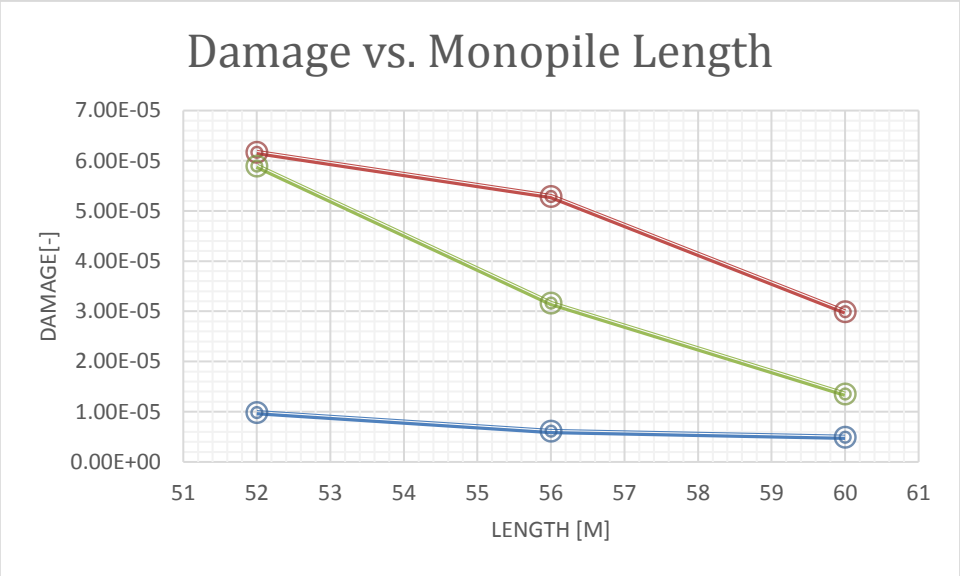

Figure 4-6 Influence of diameter in damage for different cases

Moreover, stress is reduced in depth as **Figure 4-1** shows. At the bottom, stresses are lower and, as the zone of maximum stress does not change because it is defined by the contact with seabed, it is expected that stress in longer monopiles will keep the tendency of decreasing with depth. Consequently, there will be a limit in which that stress will be 0 (or close to 0 as gravity loads will always be in the bottom of the structure) or the stresses created by lateral loading and the momentum will be 0 (the momentum is decreases also in depth due to soil influence). Therefore, longer than this limit length monopiles do not make sense as stability is already guaranteed and it would not improve fatigue behaviour too much (at least without increasing material used on the monopile and its cost substantially. Finally, installation of longer monopiles could also be more expensive and time consuming, apart from the technical problems.

5 Conclusions

From the analysis carried out it can be deduced that the location of the wind turbine is really important in terms of fatigue behaviour. Since it is directly related to the environmental loads, locations with more extreme weather will suffer higher wind speed and wave heights. This means greater loads, which make bigger damage to the structure and, consequently, its lifetime is shorter.

Moreover, in a real scenario, a structure would suffer cyclic wind loading due to gusts shorten the lifetime as a result.

Another conclusion deduced from the study is that, if the same monopile structure not introduced in the soil had suffered the same loadings, the damage would have been 60 times higher (1.6 years lifetime). Therefore, the influence of the soil in fatigue behaviour is undeniable and, as the analyses show, the soil type is also important. This is because the soil is holding the structure and more rigid soils make the structure work less, transmitting loads to the soil more efficiently. In the same way, the environment in which the monopile is placed is also crucial. Results show that the cathodic protection is indispensable.

Finally, larger monopiles (thicker, longer and/or larger diameter) suffers lower stress ranges, reducing damage and increasing lifetime.

REFERENCES

[1] W. G. Versteijlen, A. V Metrikine, J. S. Hoving, E. H. Smid, and W. E. De Vries, “Estimation of the vibration decrement of an offshore wind turbine support structure caused by its interaction with soil,” *Delft Univ. Technol.*, 2011.

[2] J. . Manwell, J. McGowan, and A. Rogers, *Wind Energy Explained: Theory, Design and Application*. 2010.

[3] D. R. Tobergte and S. Curtis, *Wind Energy Handbook*, vol. 53, no. 9. 2013.

[4] J. Van der Tempel, *Design of Support Structures for Offshore Wind Turbines*, no. april. 2009.

[5] C. L. Bakmar, “Design of Offshore Wind Turbine Support Structures: Selected topics in the field of geotechnical engineering,” 2009.

[6] X. Meng and R. Shi, “Multi-criteria assessment of offshore wind turbine support structures based on dynamic property optimization,” *High Technol. Lett.*, vol. 20, no. 4, pp. 421–428, 2014.

[7] F. Manwell, “The International Design Standard for Offshore Wind Turbines: IEC 61400-3 J.” 2013.

[8] R. Brincker, P. H. Kirkegaard, P. Andersen, and M. E. Martinez, “Damage Detection in an Offshore Structure,” 1994.

[9] P. Wirsching and Y. Chen, “Considerations of probability-based fatigue design for marine structures,” *Mar. Struct.*, vol. 1, no. October 1987, pp. 31–43, 1988.

[10] O. S. Salawu, “Detection of structural damage through changes in frequency: a review,” *Eng. Struct.*, vol. 19, no. 9, pp. 718–723, 1997.

[11] Iowa State University, “Palmgren-Miner Rule,” pp. 1–3, 2009.

[12] G. Lloyd, “Regulation of the Certification of Wind Energy Conversion

Systems, Rules and Regulations IV: Non Marine Technology Part 1," *Wind Energy*, pp. 1–480, 2005.

[13] Garcia G. G, "Design and Calculus of the Foundation Structure of an Offshore Monopile Wind Turbine," p. 101, 2012.

[14] B. Solana Santillana, "Diseño de cimentaciones de gravedad para eólica offshore," 2015.

[15] N. Stavridou, E. Efthymiou, S. Gerasimidis, and C. C. Baniotopoulos, "Investigation of stiffening scheme effectiveness towards buckling stability enhancement in tubular steel wind turbine towers," *Steel Compos. Struct.*, vol. 19, no. 5, pp. 1115–1144, 2015.

[16] L. Bauer, "Wind-turbine-models.com," 2016. [Online]. Available: http://en.wind-turbine-models.com/turbines/768-gamesa-g132-5.0mw.

[17] M. O. . Hansen, "Aerodynamics of Wind Turbines," *Routledge Taylor Fr. Gr.*, pp. 1–189, 2015.

[18] O. T. Report, "Wind and wave frequency distributions for sites around the British Isles," 2001.

[19] S. Bhattacharya, T. Carrington, and T. Aldridge, "Observed increases in offshore pile driving resistance," *Proc. Inst. Civ. Eng. Geotech. Eng.*, vol. 162, no. 1, pp. 71–80, 2009.

[20] Geotechdata.info, "Angle of Friction." 2013.

[21] Geol 616, "Some Useful Numbers on the Engineering Properties of Materials (Geologic or Otherwise)," 2000.

[22] G. Bir and J. M. Jonkman, "Modal Dynamics of Large Wind Turbines with Different Support Structures," *Int. Conf. Offshore Mech. Arct. Eng.*, vol. 6, no. July, pp. 669–679, 2008.

[23] ANSYS, "Lecture 8 Mesh Quality Introduction to ANSYS Meshing What you will learn from this presentation," pp. 1–31, 2014.

[24] DNV, “DNV-OS-J101 Design of Offshore Wind Turbine Structures,” *May*, no. May, pp. 212–214, 2014.

[25] DNV, “Design of Offshore Wind Turbine Structures,” no. February, 2004.

[26] L. De Vos, J. De Rouck, P. Troch, and P. Frigaard, “Empirical design of scour protections around monopile foundations. Part 2: Dynamic approach,” *Coast. Eng.*, vol. 60, no. 1, pp. 286–298, 2012.

[27] L. Arany, S. Bhattacharya, S. J. Hogan, and J. H. G. Macdonald, “Dynamic soil-structure interaction issues of offshore wind turbines,” *Proc. 9th Int. Conf. Struct. Dyn. EURODYN 2014*, no. July, pp. 3611–3618, 2014.

[28] T. Nishino, “BEM models for HAWT,” *Dyn. Fluid. Energy Devices*, 2015.

[29] J. Jonkman, S. Butterfield, W. Musial, and G. Scott, “Definition of a 5-MW reference wind turbine for offshore system development,” *Contract*, no. February, pp. 1–75, 2009.

[30] W. Carswell, S. R. Arwade, A. T. Myers, and J. F. Hajjar, “Reliability analysis of monopile offshore wind turbine support structures,” *Safety, Reliab. Risk Life-Cycle Perform. Struct. Infrastructures*, p. 223, 2013.

[31] T. G. Lewis, R. P. Darken, T. Mackin, and D. Dudenhoeffer, “Model-based risk analysis for critical infrastructures,” *Crit. Infrastruct. Secur. Assessment, Prev. Detect. Response*, vol. 54, pp. 3–19, 2012.

[32] M. G. Llado, “Structural Reliability Analysis and Robust Design of Offshore Wind Turbine Support Structures,” no. June, 2015.

APPENDICES

Appendix A Loading

A.1 Normal Wind Profile on Tower Bodies

Graph A-1 shows the example in *2.1.1 Wind Profile* (wind speed at 10 m 15 m/s), but the wind velocity profile is calculated for the elements in the tower (number 1 on the tower base).

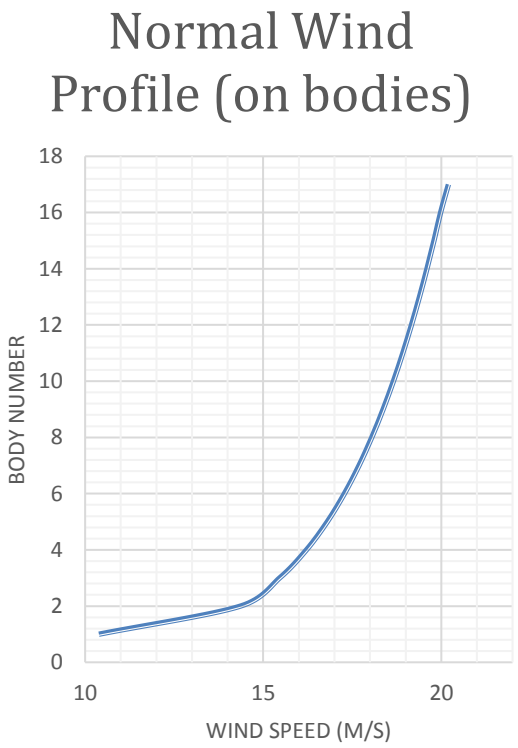

Graph A-1 NWP on tower bodies.

A.2 Wind Load on Rotor-Nacelle Assembly (BEM)

Load on the rotor is calculated according to BEM (Blade Element Momentum) theory [28]. This is an iterative process which determines forces shown in **Figure A-1**:

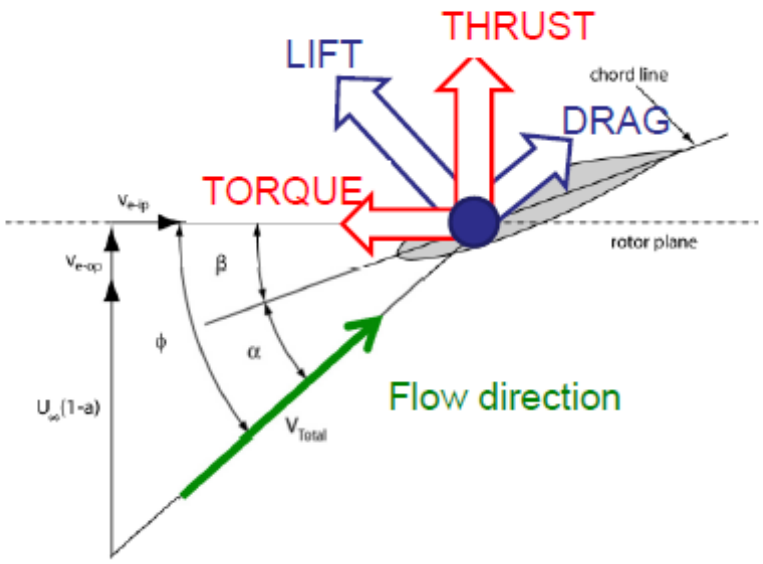

Figure A-1 Forces on the blade. [28]

In order to determine thrust (dT) and torque (dQ) for each element 5 equations must be used:

- Equation 1, determination of inflow angle (φ):

$$\tan\phi = \frac{U_\infty\,(1-a))}{\Omega\, r\,(1+a')} \qquad \textbf{(A-1)}$$

Where

U_∞: $upstream\ wind\ speed\ at\ hub\ height\ [m]$

a: $axial\ induction\ factor\ [-]$

a': $tangential\ induction\ factor\ [-\ ]$

Ω: $angular\ velocity\ [rad/s]$

r: $radius, measured\ to\ the\ mid\ of\ the\ element\ analyzed$

- Equations 2 & 3, thrust [N] and torque [N/m] generated in each blade for a dr long element (taken from blade element theory):

$$dT = \frac{B}{2}\,\rho\,{V_{tot}}^2\,(C_L\,\cos\phi + C_D\,\sin\phi)\,c\,dr \qquad \textbf{(A-2)}$$

$$dQ = \frac{B}{2}\,\rho\,{V_{tot}}^2\,(C_L\,\sin\phi - C_D\,\cos\phi)\,c\,r\,dr \qquad \textbf{(A-3)}$$

Where

$B: number\ of\ blades$

$\rho: air\ density\ [1.225\ kg/m^3]$

$V_{tot}: blade - air\ relative\ velocity\ [m/s]$

$C_L, C_D: lift\ and\ drag\ coefficents\ [-]$

$c: chord\ length\ [m]$

- Equations 4 & 5, to calculate induction factors (taken from momentum theory):

$$dT = 4\,\pi\,r\,\rho\,{U_\infty}^2\,(1-a)\,a\,dr \quad (4)$$

$$dQ = 4\,\pi\,r^3\,\rho\,U_\infty\,\Omega\,(1-a)\,a'\,dr \quad (5)$$

These five equations are used in the iterative process required to determine the total thrust on the rotor. Procedure for each element:

1. Initial estimations: $a = 0.5$ and $a' = 0$
2. Determine φ from Equation 1
3. Determine the angle of attack for the airfoil, $\alpha = \phi - \beta$
4. Look up C_L and C_D for that α
5. Calculate thrust and torque (Equations 2 & 3)
6. Use Equations 4 & 5 to update a and a' estimations
7. Repeat step 2 to 6 until induction factors converge

Then integrate dT and dQ for the whole element (1.5 m height element). β, c, r, C_L and C_D are the ones shown in the next tables.

β and c depend on r, which is the radius measured from the hub center to the middle of the element analyzed. Their values are the ones in **Table A-1**. Data is taken from [29].

element	r [m]	β [°]	c [m]
1	2.25	13.308	3.542
2	3.75	13.308	3.642827
3	5.25	13.308	3.814048
4	6.75	13.308	3.985691
5	8.25	13.308	4.157461

6	9.75	13.308	4.32871
7	11.25	13.308	4.499927
8	12.75	13.181	4.580171
9	14.25	12.52	4.614927
10	15.75	11.561	4.649683
11	17.25	10.932	4.585756
12	18.75	10.512	4.51478
13	20.25	9.9524	4.442707
14	21.75	9.672	4.366244
15	23.25	9.11	4.28978
16	24.75	8.822	4.207683
17	26.25	8.233	4.119146
18	27.75	7.932	4.03061
19	29.25	7.321	3.937512
20	30.75	7.016	3.842756
21	32.25	6.711	3.748
22	33.75	6.122	3.658
23	35.25	5.546	3.568
24	36.75	5.2585	3.478
25	38.25	4.971	3.388
26	39.75	4.401	3.298
27	41.25	3.834	3.208

28	42.75	3.583	3.118
29	44.25	3.332	3.028
30	45.75	2.89	2.938
31	47.25	2.503	2.848
32	48.75	2.3095	2.758
33	50.25	2.116	2.668
34	51.75	1.73	2.578
35	53.25	1.342	2.488
36	54.75	1.148	2.398001
37	56.25	0.76	2.306082
38	57.75	0.574	2.181507
39	59.25	0.319	1.98993
40	60.75	0.178	1.578202
41	62.25	0.062	1.166473

Table A-1 β and c for each r.

C_D and C_L were taken after a simulation on *XFLR5* for a NACA 0018 airfoil:

α [°]	**C_D [-]**	**C_L [-]**
-28	0.231704	-1.176218
-27	0.216216	-1.176686
-26	0.197269	-1.192717
-25	0.181918	-1.194815
-24	0.165205	-1.205141

-23	0.147833	-1.220527
-22	0.128266	-1.254483
-21	0.108456	-1.29349
-20	0.089368	-1.332257
-19	0.068453	-1.391157
-18	0.053545	-1.411824
-17	0.041509	-1.416976
-16	0.033183	-1.397193
-15	0.026698	-1.367914
-14	0.022314	-1.322822
-13	0.019191	-1.269097
-12	0.016981	-1.214333
-11	0.01581	-1.206325
-10	0.014164	-1.098207
-9	0.012591	-0.9663573
-8	0.011171	-0.8412838
-7	0.010061	-0.7396227
-6	0.009172	-0.6410722
-5	0.008466	-0.5381669
-4	0.007944	-0.4326866
-3	0.007587	-0.3257327
-2	0.007349	-0.2176685

-1	0.007226	-0.1090954
0	0.007187	2.77E-09
1	0.007226	0.1090971
2	0.007349	0.2176756
3	0.007587	0.3257488
4	0.007944	0.4327157
5	0.008466	0.538213
6	0.009172	0.6411395
7	0.010062	0.7397122
8	0.011171	0.8413881
9	0.01259	0.966505
10	0.014162	1.098409
11	0.015805	1.20631
12	0.016975	1.21472
13	0.019183	1.269796
14	0.022298	1.323822
15	0.026666	1.369306
16	0.033117	1.399165
17	0.041433	1.419212
18	0.053393	1.414956
19	0.068293	1.394561
20	0.089319	1.335075

21	0.108278	1.297547
22	0.128205	1.258042
23	0.147887	1.223759
24	0.165395	1.208063
25	0.182257	1.197506
26	0.197803	1.195099
27	0.217035	1.179122
28	0.232713	1.179059
29	0.264372	1.1506955
30	0.315403	1.122332
31	0.339921	1.0939685
32	0.359347	1.065605
33	0.366435	1.092194
34	0.348093	0.86233885
35	0.329751	0.6324837
36	0.34365	0.6363799
37	0.352398	0.6435987
38	0.358583	0.6513171
39	0.374237	0.651546
40	0.380798	0.656144
41	0.389284	0.6582629
42	0.401808	0.6582162

43	0.407059	0.659528
44	0.415067	0.6584217
45	0.425988	0.6561908
46	0.430179	0.6543181
47	0.435176	0.6508508
48	0.445613	0.6459552
49	0.448943	0.6411606
50	0.449357	0.6355934
51	0.458168	0.6280812
52	0.462157	0.6207075
53	0.461593	0.6126805
54	0.462689	0.6034226
55	0.468402	0.5937054
56	0.467351	0.5835131
57	0.463435	0.5726807
58	0.464452	0.5608434
59	0.465558	0.5489532
60	0.460979	0.5364745
61	0.453767	0.5234285
62	0.45535	0.5098184
63	0.45106	0.4960387
64	0.44321	0.4818891

Table A-2 C_D and C_L coefficients.

A.3 Environmental Data & Loading Validation

This part shows some data related to the Validation of processed environmental data and applicable load validation.

In order to validate the calculus performed to get the loads on the structure, same tower as in [14] was analysed (20m high) and results contrasted. **Table A-4** shows a very similar wind profiles and force results. The differences in the results are due to the power law coefficient (α) as stated before. If same α was used, the difference would be %0.00 for all the heights.

Regarding wave and current loading, results are equal to those in [14]. Wave, wind and current data introduced were also the same. **Table A-3** shows forces on the monopile for 8 wave phases are the same. Furthermore, thrust results for 8.02 m/s wind speed are also shown and compared to the result in [13].

	Total Morison Forces [MN] on the Monopile								Thrust [MN]
	α=0	α = π/4	α = π/2	α = 3π/4	α = π	α = 5π/4	α = 3π/2	α = 7π/4	
Reference Papers	4.38	32.41	41.95	28.34	-1.43	-29.83	-41.82	-27.85	0.49
Thesis	4.38	32.41	41.95	28.34	-1.43	-29.83	-41.82	-27.85	0.46
Difference [%]	0.00	0.00	0.00	0.00	0.00	0.00	0.00	0.00	6.12

Table A-3 Thrust & On Monopile force validation

After compared results with reference papers validation is successfully accomplished.

Z [m]	**Wind Speed [m/s]**			**Force on the Tower [N]**		
	U_{ref}	U	Dif. [%]	F_{ref}	F	Dif. [%]
20	32.60205	33.05715	1.395948	4691.186	4823.073	2.811383
19	32.40199	32.82062	1.291983	4679.219	4800.91	2.600658
18	32.19244	32.57312	1.18251	4663.737	4774.687	2.379004
17	31.97239	32.31351	1.066908	4644.429	4744.061	2.145199
16	31.74064	32.04041	0.944439	4620.936	4708.632	1.897798
15	31.49577	31.75222	0.814227	4592.837	4667.933	1.635084
14	31.23609	31.447	0.675214	4559.632	4621.414	1.354987
13	30.95954	31.12242	0.526108	4520.726	4568.419	1.054983
12	30.66359	30.77561	0.365309	4475.396	4508.154	0.731952
11	30.34509	30.40299	0.190802	4422.751	4439.645	0.381968
10	30	30	0	4361.675	4361.675	0
9	29.62309	29.56073	0.210499	4290.738	4272.693	0.420555
8	29.20734	29.07728	0.445293	4208.058	4170.665	0.888603
7	28.74306	28.53875	0.710812	4111.087	4052.851	1.416571
6	28.21626	27.92945	1.01645	3996.222	3915.396	2.022569
5	27.60563	27.22557	1.37673	3858.104	3752.604	2.734505
4	26.87624	26.38819	1.815892	3688.177	3555.446	3.598809
3	25.96425	25.34651	2.379186	3471.294	3308.082	4.701767
2	24.73118	23.94779	3.167621	3175.878	2977.865	6.234905
1	22.75733	21.73308	4.500741	2711.569	2472.98	8.798916
0	0	0	0	0	0	0

Table A-4 Comparison of the Wind Speed & Wind speed generated forces on the tower

Appendix B The Model

B.1 Soil –Monopile Interaction

Soil-monopile behaviour is one of the most important aspect during simulations. Soil clearly affects fatigue damage, consequently, its correct simulation happens to be crucial. Although in this paper the way of simulating it is by a large cylinder, there are many other ways to do so (usually through the application of springs and dampers). Here there are some of them:

- **Reference** [30]**:** Monopile contact with soil and their its behaviour it is simply simulated by springs (only lateral resistance).

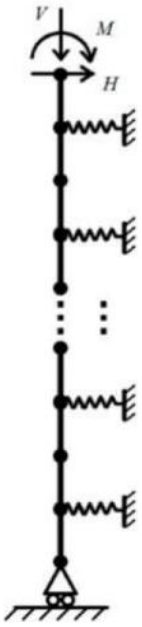

Figure B-1 Monopile-soil interaction model according to [30]

- **Reference** [31]**:** Both lateral and vertical resistance produced by the soil are simulated.

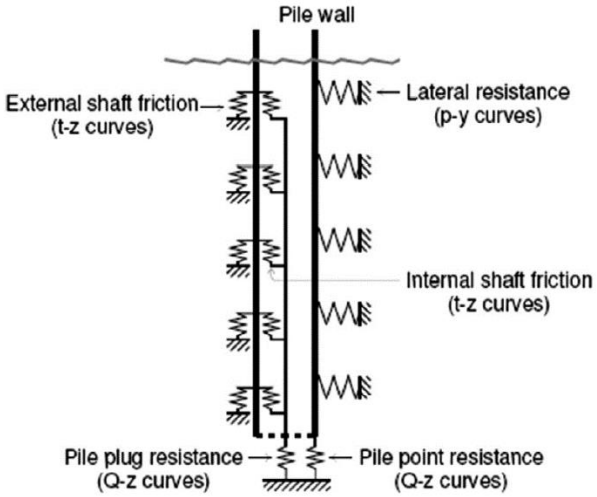

Figure B-2 Monopile-soil interaction model according to [31]

- **Reference** [32]**:** Tower-monopile structure is modelled with discrete masses and soils lateral resistance with springs.

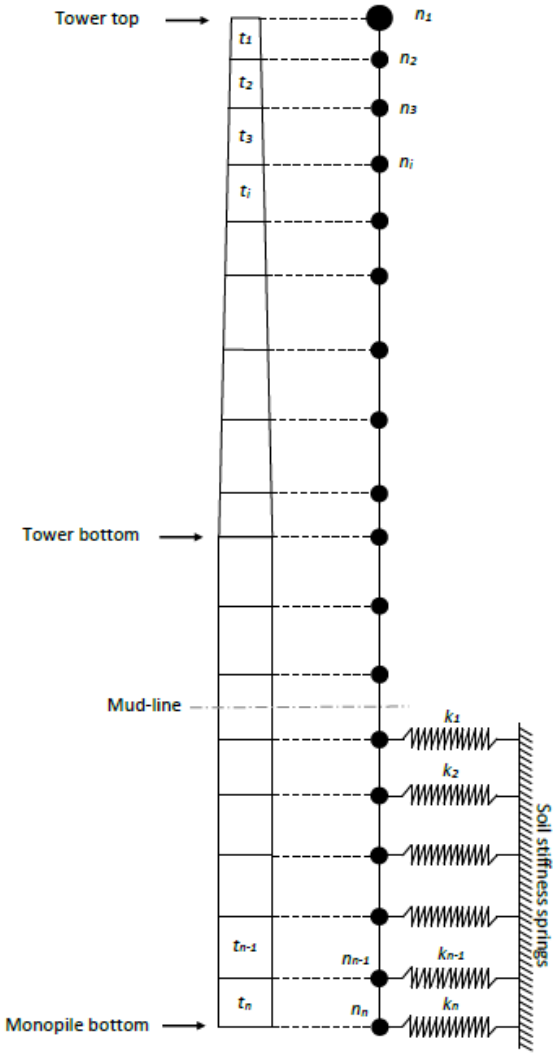

Figure B-3 Monopile-soil interaction model according to [32]

- **Reference** [1]**:** this is a more complex model as wind turbine and transition piece are also simulated. Moreover, water-monopile and soil-monopile interactions are simulated by springs and dampers.

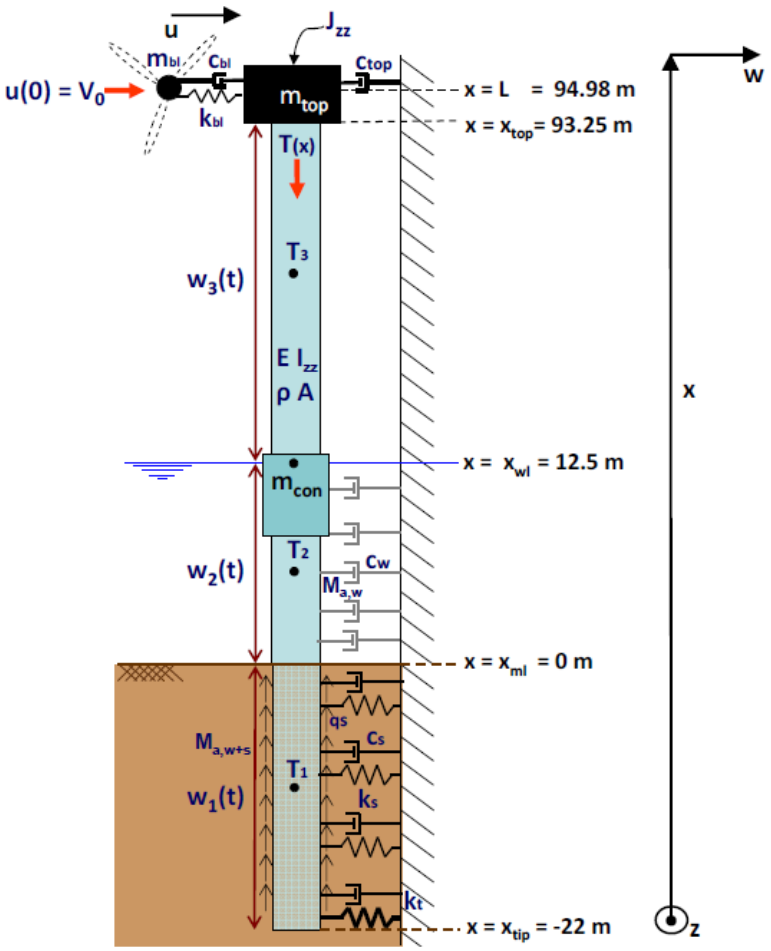

Figure B-4 Monopile-soil interaction model according to [1]

B.2 Tower Thickness

Table B-1 shows thickness of each tower element:

	Body	Thickness (m)
top	1	0.019
	2	0.019444
	3	0.019889
	4	0.020333
	5	0.020778

	6	0.021222
	7	0.021667
	8	0.022111
	9	0.022556
	10	0.023
	11	0.023444
	12	0.023889
	13	0.024333
	14	0.024778
	15	0.025222
	16	0.025667
	17	0.026111
bottom	18	0.027

Table B-1 Tower thickness for each body.

B.3 Mesh Validation

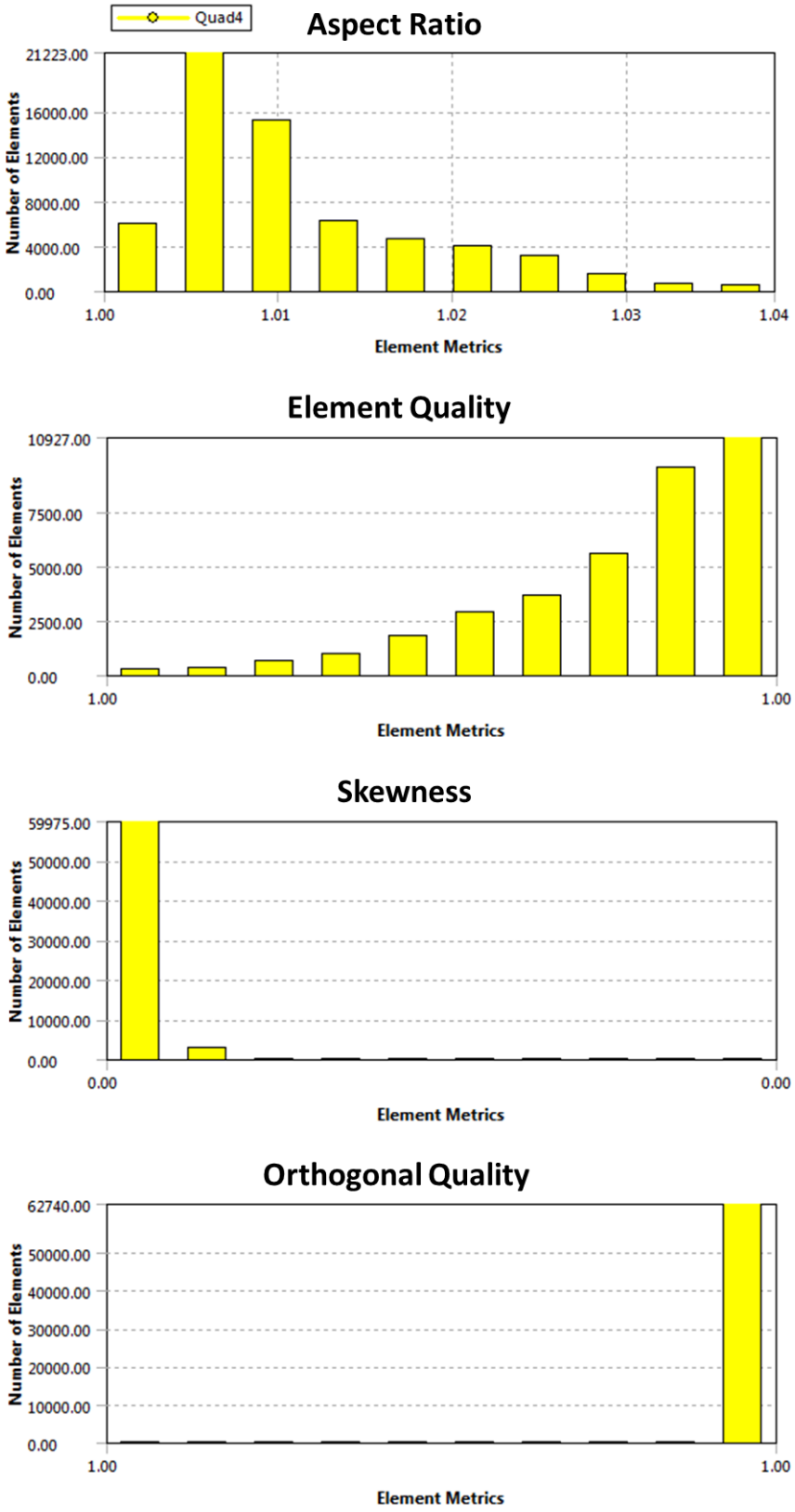

Figure B-5 Graphics of Mesh Quality related parameters

Figure B-5 **Graphics of Mesh Quality related parameters**Figure B-5 shows the properties related to mesh quality for the tower and monopile elements when its size is 0.2m. Values are OK as stated earlier in this papers. Same happens with other element sizes, although the tinier, the better the results obtained.

B.3.1 Modal Analyses

This part aims to give more information about the modal analyses described in *3.3.1 Modal Analyses*. For the modal analysis of the tower without the head mass, 1st modal frequency should be 0.8913 Hz [22]. If compared to results obtained, the difference converges to a 0.0175 Hz, which means an error of 2% as **Figure A-1**.

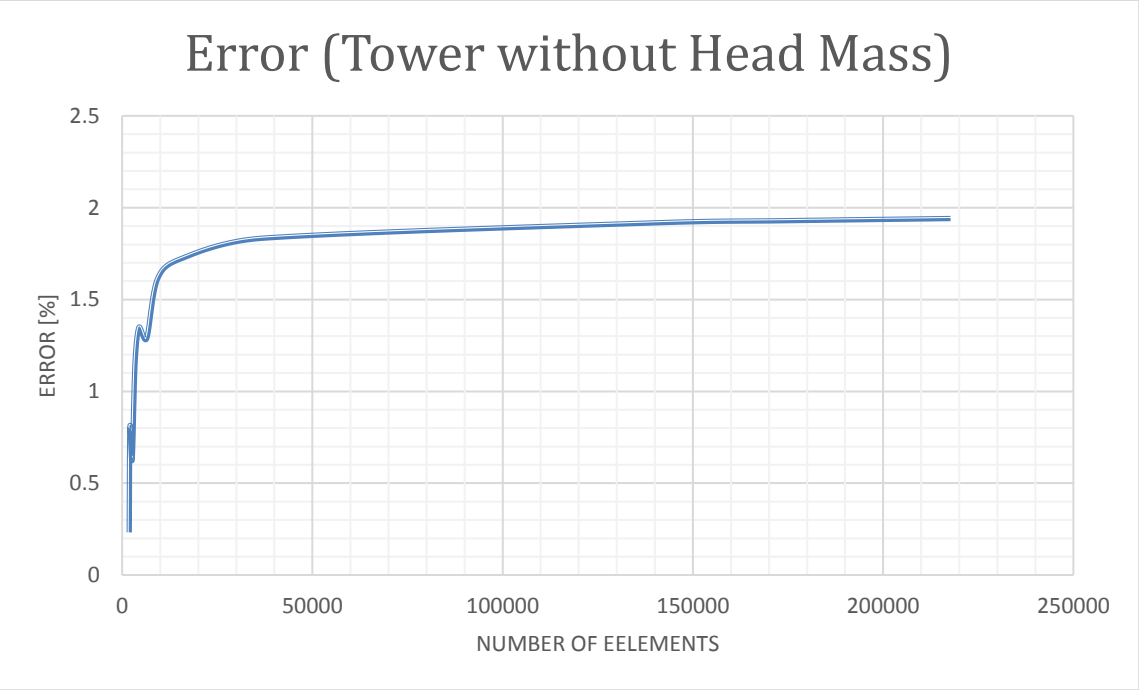

Figure B-6 Error obtained while comparing the 1st modal frequency of the model (Tower without Head Mass) with the reference paper

The error in the 1st modal frequency while the whole model is analysed (structure + soil) is a bit higher and converges to 0.2361 Hz, quite close to 0.2457 Hz [22] (a difference of 0.00963 Hz). **Figure B-7** shows this error which get values lower than 4%.

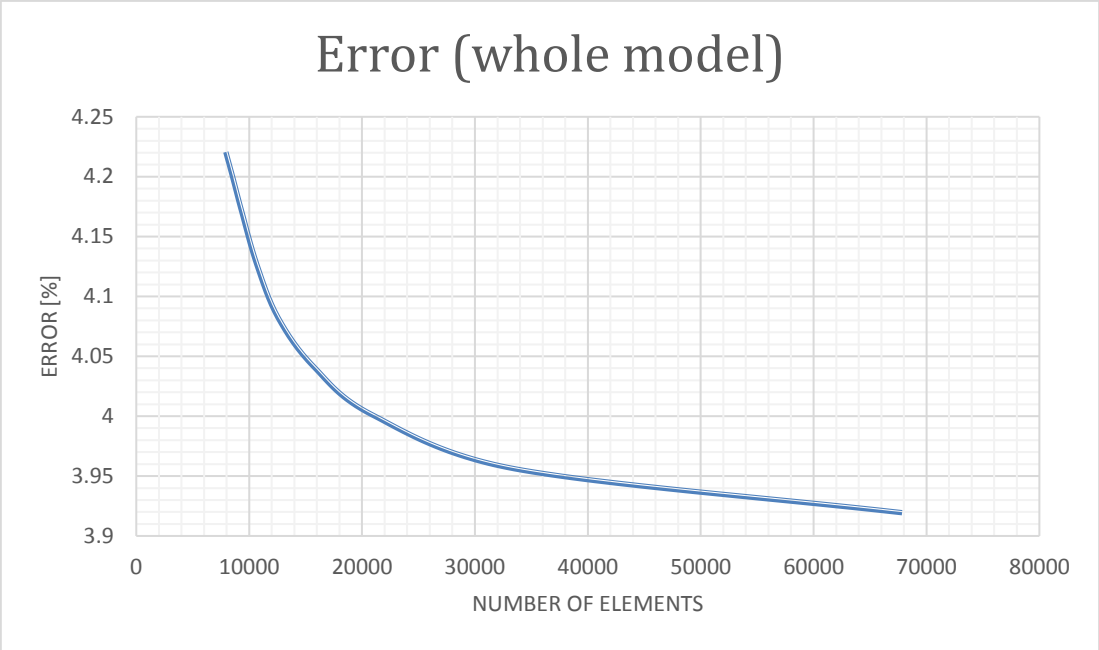

Figure B-7 Error obtained while comparing the 1st modal frequency of the whole model with the reference paper